School of Mechanical and Manufacturing Engineering

Faculty of Engineering

UNSW Sydney

Medical Image Reconstruction For Modelling Stented Coronary Phantoms

BY

Matilda Marriott

Thesis submitted as a requirement for the degree of Bachelor of Engineering in Mechatronic Engineering

Submitted: 7th August 2020   Student zID: z5191060
Supervisor: Dr Susann Beier (UNSW)

M Marriott, Undergraduate Thesis

ORIGINALITY STATEMENT

'I hereby declare that this submission is my own work and to the best of my knowledge it contains no materials previously published or written by another person, or substantial proportions of material which have been accepted for the award of any other degree or diploma at UNSW or any other educational institution, except where due acknowledgement is made in the thesis. Any contribution made to the research by others, with whom I have worked at UNSW or elsewhere, is explicitly acknowledged in the thesis. I also declare that the intellectual content of this thesis is the product of my own work, except to the extent that assistance from others in the project's design and conception or in style, presentation and linguistic expression is acknowledged.'

Signed _____

Date   07/08/2020
_____

M Marriott, Undergraduate Thesis

Abstract

Coronary Artery Disease (CAD) leads to 7.5 million deaths annually. The most common form of treatment is stenting, however the implantation of stents has been proven to cause further complications and lead to thrombosis and restenosis. Anatomically correct computational models of stented arteries can be used to better understand these failure modes. The alignment method for modeling a stented blood vessel developed by Bakiris in 2018 was replicated and critically analysed for improvements. A revised alignment method was developed, introducing several new additions to alleviate any manual intervention in the alignment process. Micro-CT reconstruction was revisited as an option for modeling stented phantoms, resulting in successful reconstruction. The process involved the implantation of the phantom with a stent, the phantom was then scanned and the micro-CT images were processed and a model was reconstructed. The final model shows some malapposition of the stent which is consistent with the micro-CT images. It was concluded that the model captured the internal geometry of the stented vessel to a greater extent than the alignment method. The reconstruction output for a stented and a non-stented phantom were used to generate Computational Fluid Dynamics (CFD) models and the CFD simulation data was used to quantify the fluid behaviour and validate the final model. The final stented output showed strong similarity to the expected behaviour of the Wall Shear Stress (WSS), Time Averaged Wall Shear Stress (TAWSS) and velocity behaviour.

M Marriott, Undergraduate Thesis

Acknowledgements

I would like to thank my supervisor Dr Susann Beier for her constructive guidance and support throughout my project. Thank you to Ramtin Gharleghi for developing the Python scripts used in the reconstruction and your ongoing guidance and input throughout the reconstruction stage of this project. Thank you to Dr Tejas Canchi for the wisdom and guidance through the meshing and CFD generation.

Thank you to Dr Nigel Jepson and Dr Kiran Sarathy from the Prince of Wales Hospital for deploying the stents in the phantoms and to Dr Tzong Tyng Hung from the UNSW Biological Resource Imaging Laboratory for performing the scans for this project.

Finally, I would like to thank my parents for their ongoing patience and support and Michael Penny for being an inspiration throughout all of my studies.

M Marriott, Undergraduate Thesis

TABLE OF CONTENTS

M Marriott, Undergraduate Thesis

M Marriott, Undergraduate Thesis

TABLE OF FIGURES

M Marriott, Undergraduate Thesis

VII

M Marriott, Undergraduate Thesis

VIII

M Marriott, Undergraduate Thesis

ABBREVIATIONS

CFD Computational Fluid Dynamics

CPD Coherent Point Drift

CAD Coronary Artery Disease

DICOM Digital Imaging and Communications in Medicine

ICP Iterative Closest Point

Micro-CT Micro Computed Tomography

NDT Normal Distribution Transform

RMSE Root Mean Squared Error

STL Stereolithography File

TAWSS Time Averaged Wall Shear Stress

WSS Wall Shear Stress

VMTK Vascular Modelling Toolkit

VTK Visual Tool Kit

M Marriott, Undergraduate Thesis

1. INTRODUCTION

Currently 7.5 million deaths occur each year as a result of Coronary Artery Disease (CAD), making it the leading cause of death worldwide [13]. Stents are small wire mesh tubes that are inserted into the blood vessel following a balloon angioplasty to open up a blocked passageway to prevent the collapsing of that blood vessel, also known as restenosis [14]. Despite being a common cause of treatment, the presence of stents have been linked to changes in the wall shear stress of the arteries due to the change in hemodynamics due to the structural changes caused by the presence of the stent [3]. Consequentially, this added stress results in damage, that in turn, causes thrombosis and restenosis, instead of preventing it.

Computational Fluid Dynamics (CFD) can be used to analyse the hemodynamic changes resulting from stent implantation, and exemplify the modes in which CAD will occur. In order to further understand the hemodynamic changes caused by stent implantation that result in CAD, producing geometrically accurate computational models of stented arteries for CFD analysis will provide further insight.

Coronary Phantoms are replicas of coronary vessels that provide a non-invasive means for conducting medical experiments. They provide the opportunity to make patient specific models; as they can both resemble the geometry of the artery and can posess the material properties [29].

Bakiris in 2018 identified a need for a computational model using phantoms to produce models of stented vessels for further CFD analysis [5]. This process was analysed and improvements to the approach were researched and deployed. Her work aimed to produce an accurate model that could be used to determine idealized stent implantation techniques for specific shaped blood vessels, and analyse the relationship between arterial shape and stent failure. The method employed point cloud registration that involved the manipulation of a vessel to take on the shape of a stent.

This study investigated and analysed the work by Bakiris critically, and improved upon the alignment method developed through her work. Improvements were made to this method by eliminating the manual alignment phase, allowing for a more reliable and replicable process.

Additionally, Micro-CT imaging and reconstruction was explored as an option for capturing the internal geometry of a stented phantom to produce models for CFD analysis. An arterial phantom underwent stenting and a model of this was produced using Micro-CT imaging and reconstruction. This model was

M Marriott, Undergraduate Thesis

subsequently deployed in a CFD simulation, yielding results that resemble the hemodynamic behaviour expected for a stented artery, indicating with confidence that the internal geometry of the phantom was captured while identifying some limitations and improvements to the modelling approach.

2

2. LITERATURE REVIEW

Coronary Artery Disease (CAD) is currently the leading cause of death worldwide [1]. A major cause of CAD are atherosclerotic lesions developing on the walls of arteries, which are commonly treated by balloon angioplasty followed by stent implantation [1]. The angioplasty consists of a balloon catheter being inserted into the artery and inflated to unblock the passage, after which a stent is then inserted to keep the artery open. The procedure allows for the opening of the blood vessel to allow blood flow to the heart [2]. The stent remains situated in the blood vessel to maintain the desired shape of the blood vessel.

Changes in hemodynamics within arteries are associated with the presence of stents; manipulating the wall shear stress of the arteries [3]. Changing blood flow and variation in shear strength damages endothelial cells; which have been linked to the cause of stent thrombosis and restenosis [4]. Beier et al. discuss the limitation of using non-deformed vessels when analysing stented blood vessels results in an overestimation of the hemodynamic parameters [3]. In order to further investigate the causes and effects of these changes in blood flow, a model of a stented vessel must be developed for further computational analysis [5]. A successful model would allow for testing the relationship between arterial shape and stent failure, as well as provide a model that can be implemented to determine ideal stent implantation techniques [5].

The work by Bakiris in 2018 produced a multiphase method that generated a stented artery model through the registration of a vessel STL file to a stent STL file [5]. The process produced a model of a vessel that registers to the shape of the stent without losing its bifurcated shape. The result was evaluated as a superior model to previous work and other alternative methods as the final model maintained the structure of both the stent and the vessel to a greater extent [5]. In terms of improvement, there should be focus into the more manual aspects of the process, allowing for less error by human judgement and a more autonomous solution. In addition to this, the final geometry should be evaluated to quantify how close to the true geometry the alignment output can be attributed.

2.1 CORONARY PHANTOMS

Arterial medical models, commonly referred to as 'phantoms', provide a model that can both reflect the geometry and the material properties of a coronary artery [29]. They provide value in that

M Marriott, Undergraduate Thesis

experimentation and implantation can be performed and the results analysed in a non-invasive manner. Due to recent developments in 3D printing technology, phantoms can be produced via 3D printing [30]. This provides a low cost and sophisticated replica of coronary arteries.

2.2 MICRO-CT IMAGING

Micro-CT (Micro Computed Tomography) is an imaging technique that involves the use of X-ray images of slices of the cross-section of the object being imaged, which combined, construct an image of the sample being scanned [31]. The image segmentation approach trialled initially by Bakiris which incorporated the use of micro-CT images was ruled out as a viable approach, as it was found that the resulting images displayed only the stent, as the resolution of the micro-CT machine used was too low to pick up both the inner lumen of the vessel and the stent concurrently [5]. Despite subjecting the captured images to a greater instance of medical imaging defects, micro-CT machines have the capability to identify both the stent and the lumen of the phantom coincidentally. The reintroduction of this technology to this method could be useful in capturing details of the inner geometry of the phantom.

An artifact, in the context of medical imaging, is any defect present on medical images. Artifacts can significantly degrade the quality of images that are captured, in many cases rendering them unusable [32]. Difficulty is often faced when imaging metallic objects in patients; the presence of metallic objects cause artifacts that can cause the readability of the images to be compromised [17]. They typically appear as streaks surrounding the metallic objects [18]. Previous studies have shown that when phantoms with deployed stents are imaged using Micro-CT, the presence of blooming and streaking artefacts results in a significant deterioration of the image quality [33]. Metallic artifacts have also proven to cause beam hardening and scatter, which result in dark streaks around the metal [34]. The presence of the metal stent causes these defects due to the high density of the material. When the density of the material is outside the range expected, it results in incomplete attenuation profiles, which causes issues in forming a correct image [32]. These artifacts can be further compounded if the calibration of the Micro-CT machine is configured without accounting for high density objects [32].

Despite being prone to these defects, it is possible for the inner diameter of phantoms to be identified using both high resolution and conventional micro-CT imaging [33]. Calibration that accounts for the

M Marriott, Undergraduate Thesis

presence of high density materials can reduce the instance of the metallic artifacts [32]. An example of this is incorporating beam hardening software during the scan to minimise artifacts.

Additionally, software corrections and post-processing of the captured images can be utilised to reduce the occurance of metallic artifacts. Interpolation techniques can be used to account for the out of range values in the attenuation profiles, however as this is an interpolation, it results in a significant reduction of detail where the metal meets the tissue [32]. Micro-CT can be implemented to capture the internal geometry of a stented phantom, but the capturing and postprocessing of the data must be optimised to account for medical imaging defects caused by metallic objects in order to avoid degredation of the geometry captured.

2.3 MODELLING DEVELOPMENT

Bakiris in 2018 developed a process that utilised image registration techniques to produce a model of a stented artery. The method involved taking the STL file of a reconstructed model of a 3D printed phantom prior to stenting and a model of a sample stent, both underwent pre-processing; the stent was downsampled and the vessel was reduced to the inner lumen geometry. Image registration, the Iterative Closest Point (ICP) and Coherant Point Drift (CPD) algorithms were applied to produce a vessel that registered to the shape of the stent. After smoothing and clipping of the registration output, the final output can be seen in figure 1.

M Marriott, Undergraduate Thesis
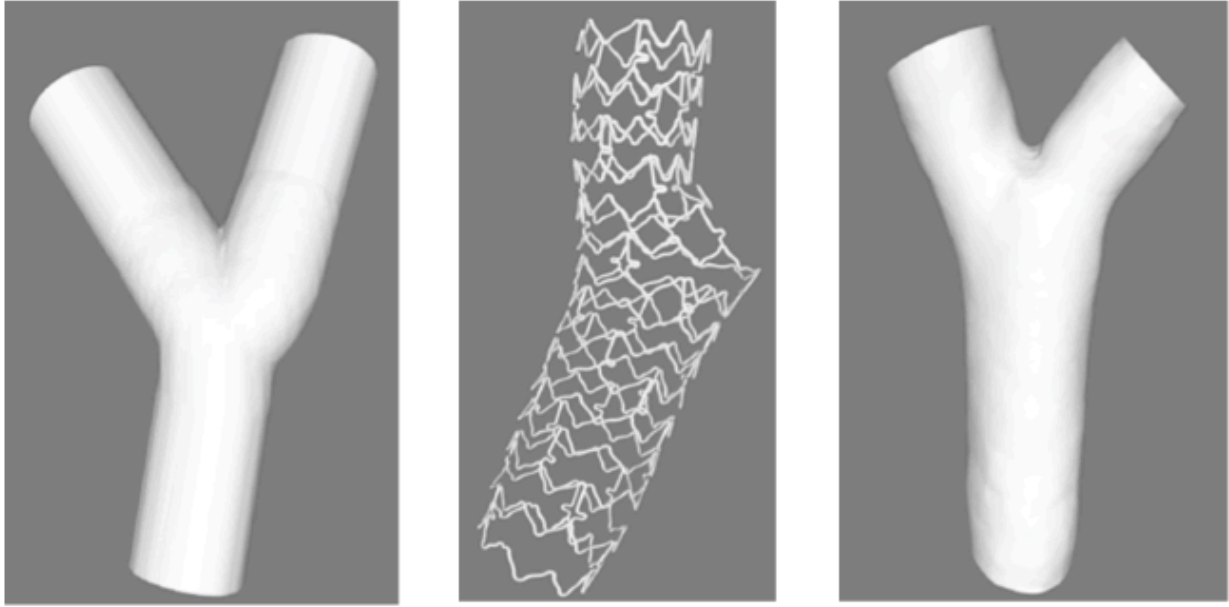
FIGURE 1 - ORIGINAL VESSEL STL FILE (1), STENT STL FILE (2), STENTED BLOOD VESSEL (3) [5]

Bakiris evaluates that the final model is of an acceptable standard; however this model was developed based on one case and is a manually intensive process that is difficult to replicate exactly. When considering a larger application to a range of data; the replication of the same steps must yield a reliable model after the use of the same steps for the process to be considered robust. The process was replicated fully to assess its usability and replicability, as the desire to apply this method on a wider sample size warrants the need to replicate it simply with little uncertainty and guesswork.

Figure 2 summarises the steps in this alignment process. The two STL files are preprocessed in preparation for alignment. The alignment consists of a manual alignment followed by an automated alignment in which the vessel is mapped to the stent. The vessel is then loaded into Meshlab for surface reconstruction and then post processed by clipping the ends of the vessel and smoothing out the final model using the Vascular Modelling Toolkit (VMTK).

M Marriott, Undergraduate Thesis

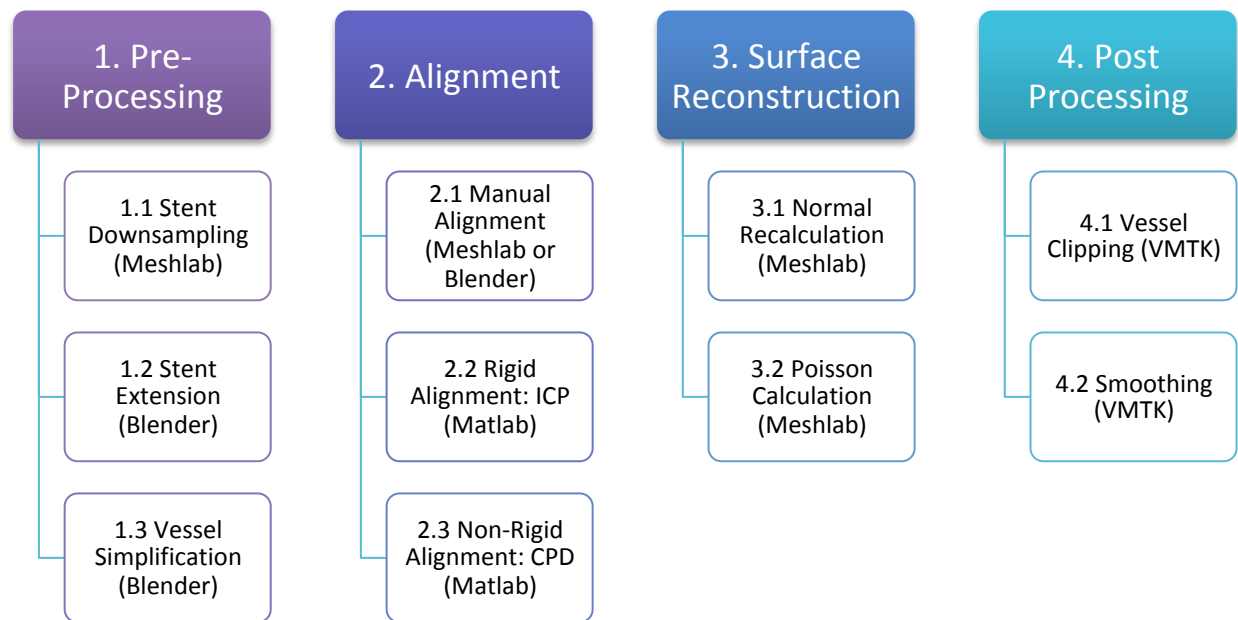| 1. Pre-Processing	2. Alignment	3. Surface Reconstruction	4. Post Processing
1.1 Stent Downsampling (Meshlab)	2.1 Manual Alignment (Meshlab or Blender)	3.1 Normal Recalculation (Meshlab)	4.1 Vessel Clipping (VMTK)
1.2 Stent Extension (Blender)	2.2 Rigid Alignment: ICP (Matlab)	3.2 Poisson Calculation (Meshlab)	4.2 Smoothing (VMTK)
1.3 Vessel Simplification (Blender)	2.3 Non-Rigid Alignment: CPD (Matlab)		

FIGURE 2 - BAKIRIS' MODELLING PROCESS [5]

2.3.1 ALIGNMENT

The three stages of alignment were chosen as they were evaluated as producing a final output that best resembled the expected geometry. This was evaluated after preliminary testing with the ICP algorithm, concluding that more stages were needed to achieve an acceptable output. [5]

The first stage in this alignment phase is importing the preprocessed STL files in the 3D modelling software Blender and ensuring that both are the correct size and orientation in relation to each other. This involves a series of scaling, rotating and translating actions to ensure the two point-clouds are close enough for the automatic sections of the registration process to occur. This process is done by the user manually applying these changes until they make the judgement that the file is orientated correctly. If the orientation of these point clouds are not aligned initially, it would cause the final vessel to be stretched or compressed more than the actual structure.

7

M Marriott, Undergraduate Thesis

Once manually aligned, rigid alignment takes place using the Iterative Closest Point (ICP) Algorithm in Matlab. This algorithm aligns the two stent and vessel point clouds without deformation. Both keep their structure but fit to reduce the mean square error between the two point clouds. Next non-rigid alignment takes place by applying the Coherent Point Drift (CPD) algorithm in Matlab, fitting the vessel to the stent to allow the vessel to take the shape of the stent.

The ICP and CPD algorithms work to achieve a model that satisfies the final constraints. As for the manual alignment; it works to align the two STL files to a standard that is considered acceptable but it involves considerable scaling, rotating and translating until the two files "look right". This is an error prone and hard to replicate process that should be automated to avoid these two major issues.

The key step in modelling a stented vessel entails both manual and automatic alignment. This is how the final vessel is constructed to match the structure of the stent. However, the initial step developed for this alignment consists of manual scaling and rotation. In order to allow consistency and universal application; it would be optimal for all alignment to be automated. Methods of automatic rigid alignment and scaling were looked into in order to make this process more automated.

As it stands, the ICP Algorithm typically cannot handle large instances of random noise; the presence of outliers or scaling between the two point sets provided [11]. The ICP algorithm is limited as it cannot perform optimally if there is significant noise, the presence of outliers or if there is significant scaling relationships between the two data sets [7]. Because of this, if the STL files for both the stent and vessel are not scaled to the correct relative size and orientation, the ICP algorithm will prove ineffective and yield a vessel that does not take the shape of the original stent nor maintain a similar original structure.

2.3.2 ALIGNMENT ALTERNATIVE APPLICATIONS

There are clear limitations to the current alignment process; the addition of new approaches to registering the point clouds can be developed and applied to decrease the guesswork and improve the performance of the Matlab registration process.

M Marriott, Undergraduate Thesis

There are many options for rigid point cloud registration that allow for translation and rotation of one point cloud to align with another. However, few of these algorithms allow for a scaling factor, which do not make them a viable replacement for the manual alignment phase. Procrustes analysis is a form of rigid registration that involves identification of landmarks on each data set and calculating the transform based on the Root Mean Square Error (RMSE). The method provides a rotation and scaling factor as well as a translation vector to register one data set to the other [8].

The implementation of this algorithm would alleviate the need for manual intervention during the alignment phase. Essentially the algorithm aims to fit the point cloud A to point cloud B. In terms of rotation, the algorithm aims to solve equation 1, where A and B are both point clouds and T is the rotation matrix [9].

$$A = TB \hspace{5cm} \text{Equation 1}$$

The problem can be further extended to solve for translation and scaling [9]. In terms of the problem we are trying to solve, these three parameters must be evaluated.

$$A = sTB + D \hspace{5cm} \text{Equation 2}$$

Given this expression, the generalised procrustes problem when minimised is expressed as in equation 3.

$$\|A - s(BT + D)\|w = \sqrt{\text{tr}((A^T - s(T^TB^T + D))W(A - s(BT + D))} \to \min_{T,s,D}, \hspace{1cm} \text{Equation 3}$$

The solution to the general procrustes problem evaluates a rotation, scaling and translation vector that aligns point cloud B to A. These outputs would be implemented to the stent point cloud to align it to the vessel prior to ICP registration.

M Marriott, Undergraduate Thesis

2.3.2.2 NORMAL DISTRIBUTION TRANSFORM

The Normal Distribution Transform (NDT) is a method of rigid registration that could be implemented in place of the ICP algorithm. The NDT performs in a similar way to ICP; it represents the point cloud as a set of Gaussian distributions that model the surface locally. It has an advantage over ICP as it does not have to search for closest neighbours as ICP does, it avoids that bottleneck and will run more efficiently [10]. The implementation of this method in place of the ICP algorithm could combat the issues faced due to crashing of the algorithm due to the stent file having more vertices.

2.4 MODEL VERIFICATION

As it stands, the method developed was concluded to be of an acceptable standard. Figure 3 shows the Stent vs Vessel similarity for the Growth and Image Segmentation techniques trialled previously by Bakiris. Stented vessels deform to take on the shape of the stent once implanted and can permanently deform the artery to this shape [6]. Therefore, to develop a realistic model, we would expect to see a vessel that registers to the shape of the stent. Figure 3 shows that for the method employed by Bakiris, labelled 'Novel Approach', the vessel shows an increase in stent similarity and a small loss in vessel similarity when compared to other approaches.
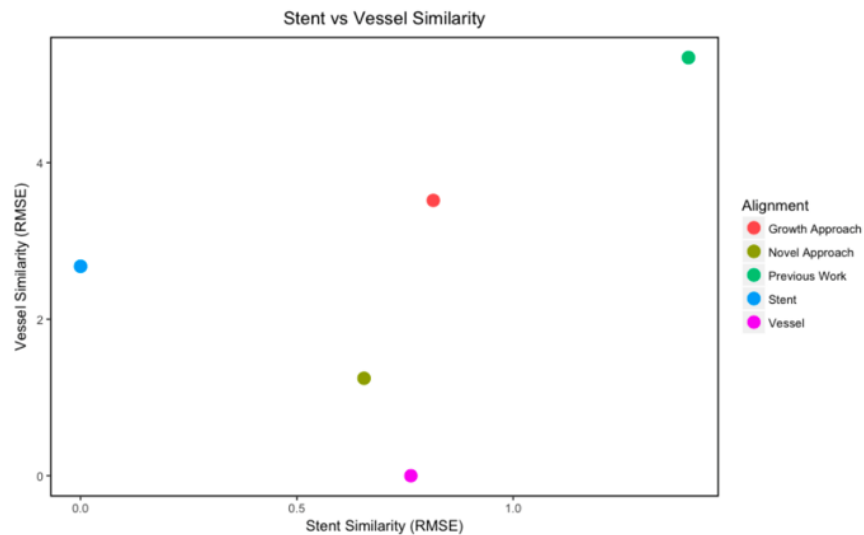

FIGURE 3 - STENT VS VESSEL SIMILARITY [5]

10

M Marriott, Undergraduate Thesis

The accuracy of the output was evaluated through the means of evaluating the RMSE between the output and the Stent and Vessel models respectively. While this was a useful approach when evaluating the relative accuracy of the different modelling approaches, it provides little insight into whether the model is a valid representation of a stented phantom. Critical geometry can be lost in all stages of the modelling approach, therefore it is important that the final model can be verified.

2.4.1 HEMODYNAMIC BEHAVIOUR OF STENTED ARTERIES

In terms of validating the model produced, a method of verification needs to be developed in order to conclude with confidence that the final model resembles the geometry of a stented phantom. Comparison of the final model with medical images can be used as an initial basis for comparison, to see if the model is representative of the position of the actual phantom and stent. However, further verification is needed to account for more subtle inconsistencies that cannot be identified visually.

Revisiting micro-CT reconstruction as a means of generating a model brings the potential error of medical imaging defects. This could result in the identification of geometry that is not present due to medical imaging artifacts around the stented region as well as increasing the surface roughness.

Computational Fluid Dynamics (CFD) can be utilized to analyse the behavior of the model. By running simulations of the model, the output can be analyzed and compared to the behavior of stented vessels and from there, it can be concluded if the model produced is representative of the geometry we would expect. The velocity, Wall Shear Stress (WSS) and Time Averaged Wall Shear Stress (TAWSS), are used as parameters to analyse the fluid behaviour and conclude the validity of the model.

2.4.1.1 VELOCITY

The velocity profile around the stented area is a metric that can be used to analyze the hemodynamic changes between the stented and non-stented models.

The flow profile throughout most of the circulatory system follows laminar flow [19]. The velocity of this flow is characterised with a parabolic profile, where the maximum velocity occurs at the centre of the flow and slowly tapers off to zero at the boundary between the fluid and the vessel wall [20]. This profile occurs due to the friction both within the fluid and between the fluid and the vessel wall and is significantly impacted by fluid viscosity [20].
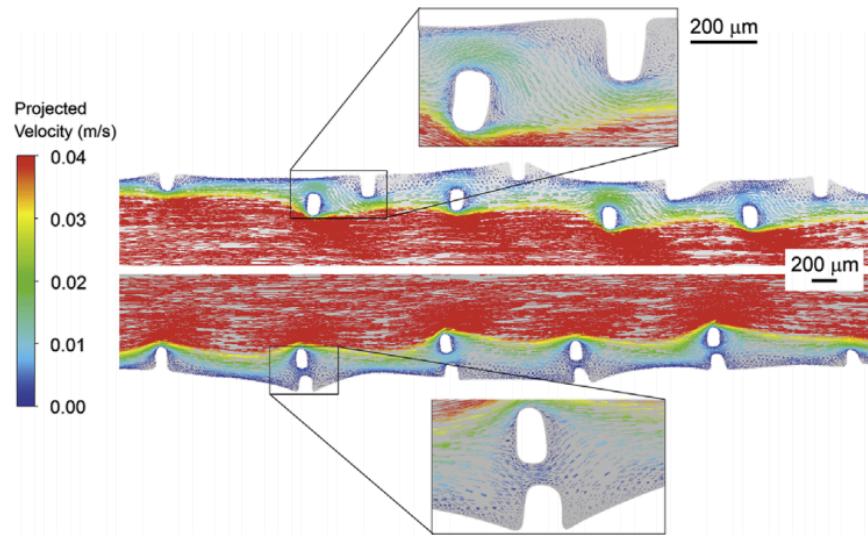
M Marriott, Undergraduate Thesis

FIGURE 4 - PROJECTED VELOCITY FOR OVERLAPPING STENT [35]

Introducing a stent introduces irregularity to that boundary layer, resulting in a distruptionto the flow in that region. Figure 5 shows a projection of streamlines in the vicinity of stent struts. When the laminar streamlines approach the strut walls, recirculation occurs, resulting in more turbulent flow behaviour. In the image on the right, where the stent struts are closer together, there is significant recirculation.
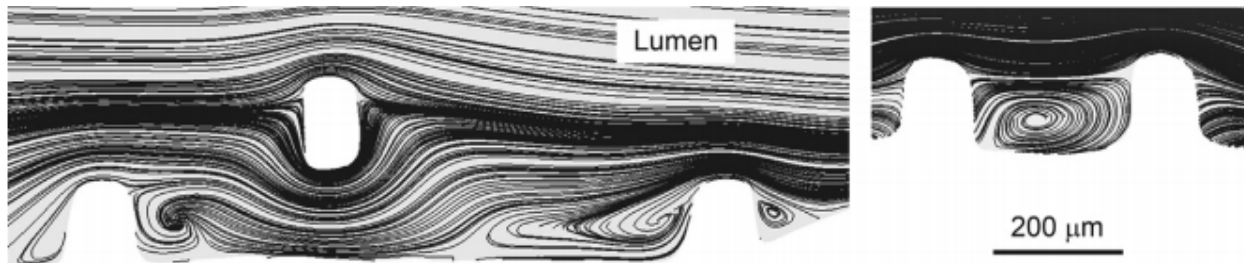

FIGURE 5 - PROJECTION OF STREAMLINES IN VICINITY OF STENT STRUTS [35]

The presence of the stent would therefore increase the turbulent flow in the vicinity of the stent. In terms of validating a final output, it can be expected that, when directly comparing the stented and non-stented region, the boundary layer will be larger in the stented region.

M Marriott, Undergraduate Thesis

The hemodynamic conditions inside blood vessels lead to shear stress applied at the inner layer of the arterial wall that is in contact with the blood [21]. There is significant evidence that areas of low or oscillatory shear stress increase the risk of atherosclerosis for the patient [22]. Wall Shear Stress (WSS) and Time Averaged Wall Shear Stress (TAWSS) are two metrics that can be used to quantify the hemodynamic changes between stented and non-stented arteries.

WSS is the force per unit area the wall exerts on the fluid in arterial blood flow [22]. TAWSS is defined in equation 4:

$$TAWSS = \frac{1}{T} \int_0^T |\vec{\tau_w}| dt \qquad \text{Equation 4}$$

Where $\vec{\tau_w}$ is the WSS vector and T is the duration of an entire cardiac cycle [23]. This metric provides a more holistic representation of the WSS distribution throughout the cardiac cycle.

In a healthy, non-stented coronary artery, the TAWSS distribution is expected is exemplified in figure 6. There will be relatively consistent TAWSS throughout the vessel; once the vessel bifurcates, the outer most regions will experience lesser TAWSS due to the bifurcation causing a lesser velocity in these regions as the highest velocity region splits off at the bifurcation point.
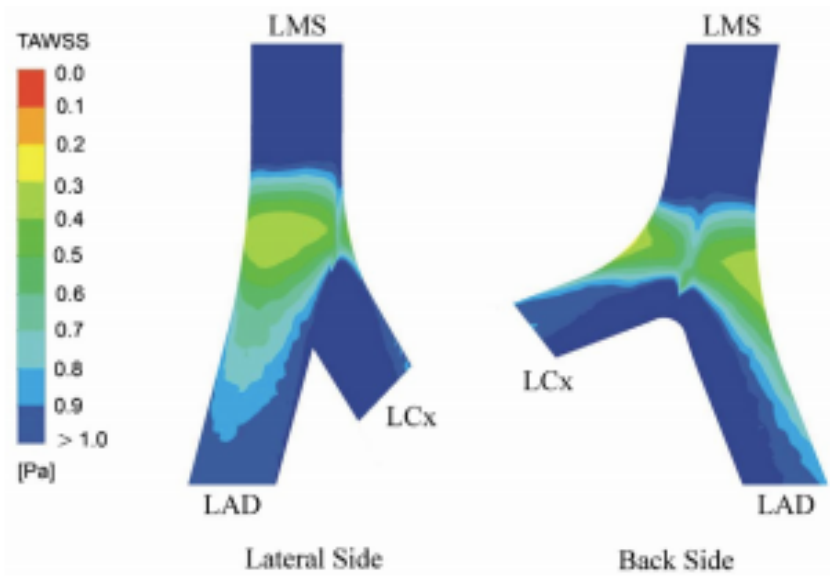
FIGURE 6 - TAWSS DISTRIBUTION IN A NON-STENTED, NON-OBSTRUCTED LEFT CORONARY ARTERY [38]

Coronary stent design has an effect on the wall shear stress on the surface of the vessel, resulting in a range of complications [25]. The presence of the stent causes hemodynamic changes which alter the WSS distribution across the surface of the vessel [26]. The interaction between the blood flow and the stent struts results in WSS variation, especially around the stent struts [27]. This variation is characterised with low WSS at the location of the stent struts.

The TAWSS distribution follows similar expected behaviour to that of the WSS. TAWSS distributions show a lower value around the location of the stent struts [24]. The presence of low shear stress is often associated with unstable flow conditions, such as turbulent flow, stagnant flow and blood recirculation [21]. As previously discussed, increased turbulent flow would be expected with the introduction of a stent; therefore this change would yield a drop in WSS.
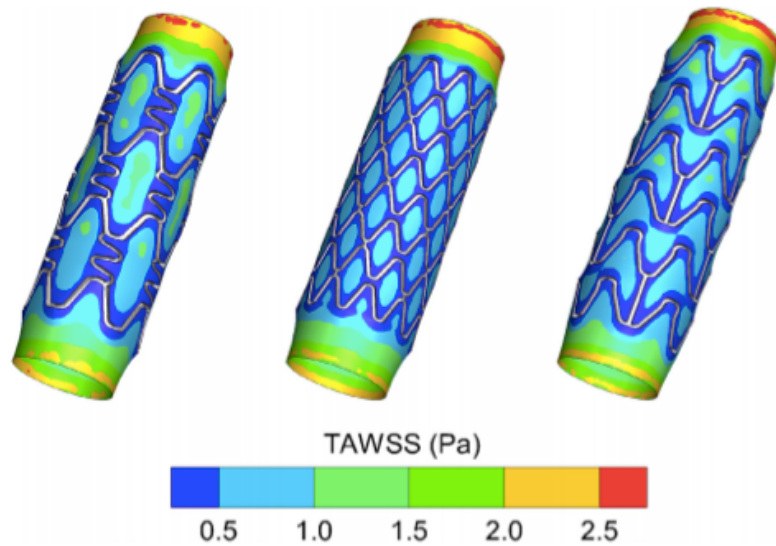
14

M Marriott, Undergraduate Thesis

FIGURE 7 - TAWSS OF STENTED VESSELS [24]

Additionally low WSS is associated with higher velocities, therefore the introduction of the stent can be characterised by increased velocity as well as a decrease in WSS and TAWSS [37]. It would be expected that the stented region of the model produced will demonstrate an increase in velocity, as well as a corresponding reduction in WSS and TAWSS, corresponding with the strut locations. If the final model demonstrates the outlined behaviour, the model can be validated further as a representation of a stented coronary artery.

15

3. METHODOLOGY

On initial reflection of the alignment method, a clear downfall to the replicability and reliability of the process was identified in the manual aspects of the process [4]. The process required sufficient manual scaling performed by the user in order for the ICP and CPD alignment to be successful. The vessel was required to be scaled, rotated and translated to align with the stent before the automatic sections of the Matlab alignment is to take place. Because there was no clearly defined way to carry out this process without multiple attempts, it was made a priority to eliminate the need for manual intervention. As a result, alternative approaches were investigated to eliminate the need for manual intervention. The manual stage was successfully replaced with an automatic scaling and alignment phase added to the matlab script for alignment. The Matlab script successfully scales and aligns vessel and stent inputs with varying sizes and configurations within limits.

In addition to improvements to the alignment method, it was decided that there was significant reason to revisit the original approach made by Bakiris to reconstruct micro-CT images of stented phantoms. A reconstructed micro-CT model will allow the capturing of the geometry directly from medical images, and could serve as a more accurate means of modelling stented phantoms.

After executing micro-CT as an alternative solution, it was evaluated that this model was a more reliable and accurate representation of a stented phantom. Previous conclusions about the feasibility of reconstructing stented phantoms were challenged, resulting in the implementation of new processing techniques that resulted in an accurate reconstruction of the stented phantom. Because of this, the ideal modelling technique has deviated from focusing on alignment techniques back onto the initial ideal approach of micro-CT reconstruction. As a further step after this validation, the reconstructed models were used to develop CFD meshes and simulations were subsequently run as a means of further evaluation of the validity of the reconstruction output.

3.1   ALIGNMENT IMPROVEMENTS

The alignment method designed by Bakiris in 2018 was evaluated and the main improvement identified for a more optimised process was the elimination of manual scaling and alignment. This process was to be replaced with an alternative means of automated rigid registration implemented within the Matlab alignment script in the revised alignment method [4].
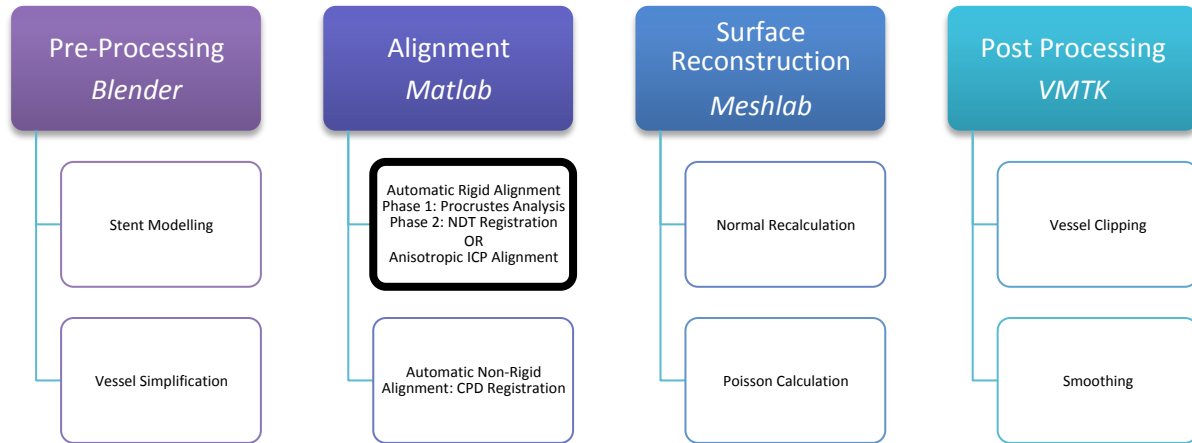

FIGURE 8 - REVISED ALIGNMENT METHOD [4]

The elimination of manual intervention was achieved by the implementation of automatic scaling and an additional rigid registration step through the addition of the NDT algorithm prior to the ICP and CPD Algorithms.

3.1.1   PROCRUSTES

The procrustes analysis was initially a main approach considered to solve the manual intervention problem. Procrustes analysis is a method of rigid registration that was concluded to allow for a greater accuracy for alignment prior to the CPD algorithm [4]. This method was concluded as the best option initially to improve the alignment. It was initially trialled as an option prior to ICP registration, but it was found that Procrustes alignment requires two point clouds to have identical numbers of points when implemented in Matlab. This would result in drastic downsampling of the stent to match the vessel. The

M Marriott, Undergraduate Thesis

Procrustes method was not implemented due to this reduction and the NDT algorithm was implemented to maintain stent resolution.

3.1.2 SCALING

From the evaluation of earlier trials, the ICP and CPD algorithms performed poorly when the relative size of the stent and the vessel did not match [4]. The algorithms did not allow for scaling of the vessel point cloud as a part of the alignment process. Therefore, it was key for the process to incorporate a means of scaling the vessel pointcloud to match the relative size of the stent to allow for successful registration.

After identifying that the objective was to match the vessel junction with the stent in terms of size, a scaling factor was calculated and applied to the vessel pointcloud to get it to match with the stent size. For the vessel to have a diameter that aligns with the stent, it was found through trial and error, that the stent would have to be approximately the same length in the z-direction as the vessel. This condition is specific to the specific models used in this example; for use on different models with varying shapes and lengths this will need to be adjusted.
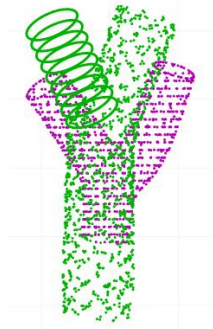

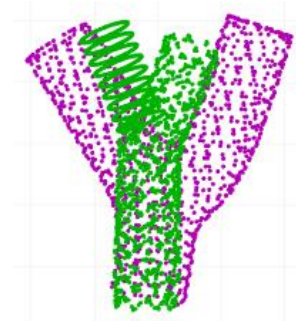FIGURE 9 - VESSEL AND STENT PRE-SCALING

FIGURE 10 - VESSEL AND STENT POST-SCALING

The range for both the vessel and stent are determined and the scaling factor is calculated from the ratio of stent range to vessel range. Each value in the vessel pointcloud is multiplied by this value to scale it to match the size of the stent.

$$Range_{Vessel} = Max_{Vessel} - Min_{Vessel} \ , Range_{Stent} = Max_{Stent} - Min_{Stent} \qquad \text{Equation 5}$$

M Marriott, Undergraduate Thesis

$$Scaling\ Factor = \frac{Range_{Stent}}{Range_{Vessel}}$$

<div align="right">Equation 6</div>

$$Scaled\ Vessel = Vessel * Scaling\ Factor$$

<div align="right">Equation 7</div>

For this method to work, both the stent and vessel must be upright and positioned aligned so that the stent is aligned with the branch of the vessel to be stented.

3.1.3 NDT ALIGNMENT

Initially, the NDT algorithm was added as a step prior to the ICP algorithm. It was found that the addition of the NDT Algorithm showed success in improving the extent of rotation and translation to align the stent with the vessel; however, it did not account for scaling, and therefore the CPD registration was unsuccessful in producing a vessel that resembled a stented blood vessel. Once it was implemented post-scaling, it allowed further alignment that alleviated the need for manual rotation and translation
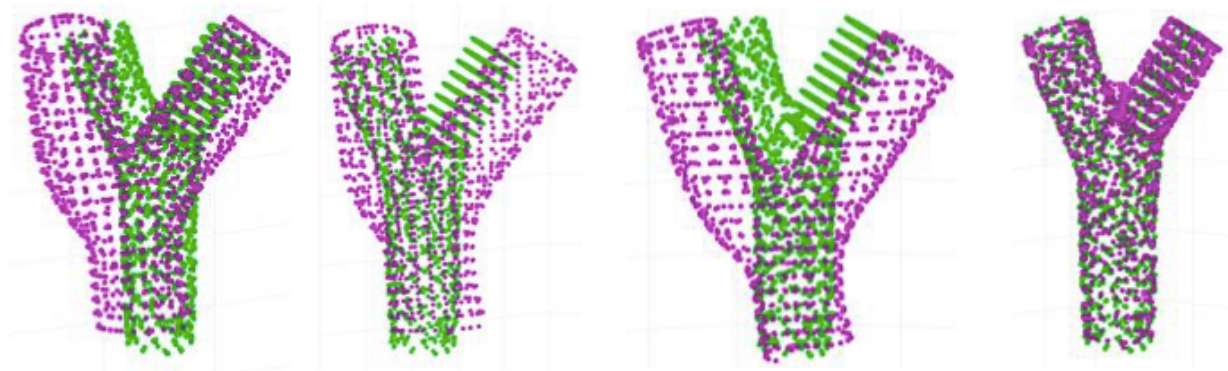

FIGURE 11 - VESSEL AND STENT POST-SCALING (1), POST NDT ALIGNMENT (2), POST ICP ALIGNMENT (3) AND POST CPD ALIGNMENT (4)

Despite the additions to the Matlab component of the process allowing successful output without significant manual intervention, this factor could not be eliminated entirely. The alignment of the vessel relative to the stent can cause incorrect alignment in three particular cases that should be avoided on input; aligning the vessel perpendicular to the Z-Axis, upside down and aligned with the incorrect branch of the bifurcation.

M Marriott, Undergraduate Thesis

When the Vessel is perpendicular to the Z-Axis, an error is caused in the scaling algorithm; as the scaling is determined by the range of points in the Y-Axis, aligning the Vessel with the Z-Axis causes this range measurement to be significantly smaller; as it is measuring the width of the vessel. This causes the scaling factor to be amplified and the vessel ends up significantly larger than the stent. An example of this can be seen in Appendix A.1.

If the vessel is input as upside down, the NDT and ICP algorithms will not rotate the vessel upright, resulting in incorrect registration. This is shown in Appendix A.2: the output bears similarity to the stent, but is inconsistent as it has manipulated the upside down vessel.

The alignment of the two input files can affects which branch of the bifurcated vessel will register to the stent. Whatever branch is closest of the vessel that is initially aligned to the stent will be the one that is registered as the NDT algorithm is aligning using the shortest distance. In order to achieve the correct branch stented, the vessel must be imported aligned towards the desired branch more so than the undesired branch. An example of this can be seen in Appendix A.3 and A.4, in which different positions of the vessel result in the stent registering to a different bifurcation.

20

M Marriott, Undergraduate Thesis

3.2   MICRO-CT RECONSTRUCTION

Micro-CT reconstruction of a stented phantom is an alternative method that can be used to capture and model the internal geometry. This was originally ruled out as an option by Bakiris as the high density of the stent did not allow for the shape of the inner lumen to be visible in the reconstruction [5]. As they are metallic objects, stents have a relatively high density [16], due to this the Micro-CT images clearly show the metal stent but show the lumen of the vessel with much lower luminosity.

As discussed in section 2.2, capturing the geometry of both the stent and the phantom is a possibility; there is added risk of medical imaging defects but these can be significantly reduced by the machine settings when capturing the images, and subsequently reduced when the images are post-processed. In preparation for this method, meetings with technicians were conducted for consultation regarding the validity of the model. Several discussions and trials with the stented model resulted in confirmation that capturing the internal geometry was a possibility and the machine was calibrated accordingly.

Initially, as a means of comparison of final stent geometry, a micro-CT scan of the phantom, pre-stenting, was performed providing 1842 DICOM images of the non-stented phantom.

The same phantom was then stented using the balloon angioplasty method by a registrar cardiologist. The phantom was laid on the operation table and the phantom was lubricated with saline solution. Using a guidewire the stent was inserted following the process of a balloon angioplasty with an X-ray as a guide to ensure correct deployment.

M Marriott, Undergraduate Thesis

FIGURE 12 - PREPARATION OF PHANTOM TO BE STENTED BY REGISTRAR CARDIOLOGIST

FIGURE 13 - LIVE X-RAY IMAGE CAPTURE OF PHANTOM BEING STENTED

The stent was then scanned by the same Micro-CT machine The output of the Micro-CT scan resulted in 1842 DICOM images of slices taken lengthwise of the stented phantom.
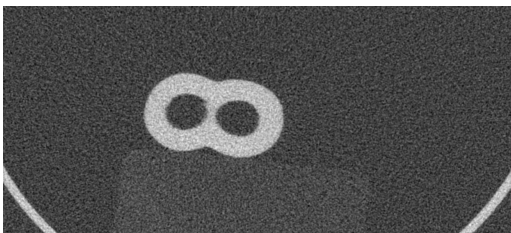

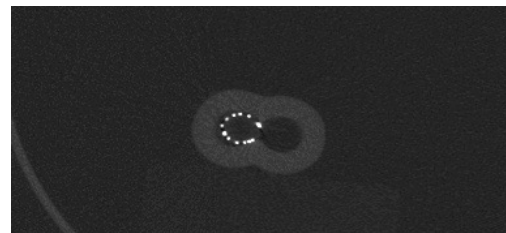**FIGURE 14 - MICRO-CT IMAGE OF NON-STENTED PHANTOM**

FIGURE 15 - MICRO-CT IMAGE OF STENTED PHANTOM

The DICOM images were processed and reconstructed using Python. The Visualisation Toolkit (VTK) is an open source software commonly used for image processing [28]. The script developed loops through all images in order, using image thresholding through VTK functions to enhance the image of the vessel lumen and stent with respect to the background of the image. This is difficult to achieve as the images with the stent present show the lumen and background, sharing an almost identical shade, so full resolution DICOM images were used, resulting in significant processing time. After the shape of the lumen and stent were identified and enhanced, the VTK STL writer object was used to write separate STL

22

M Marriott, Undergraduate Thesis

files, one of the stent and the other of the vessel. The two are distinguishable as the luminosity of the stent is significantly greater than that of the vessel, so the thresholding allows for the identification of separate objects.

The two STL outputs were combined to produce the final model. The final model produced is a high resolution model of the stented phantom from the DICOM data. The same procedure was carried out for the reconstruction of the non-stented model.
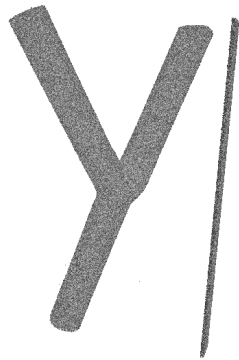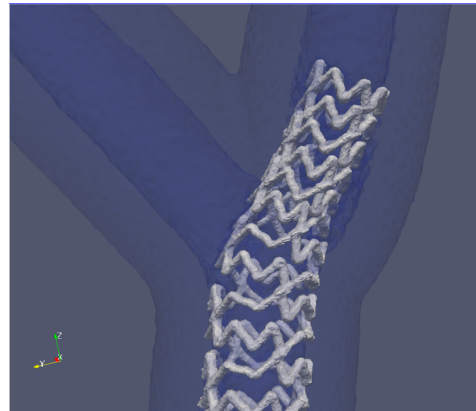

FIGURE 16 - RECONSTRUCTED MODEL OF STENTED PHANTOM

FIGURE 17 - RECONSTRUCTED MODEL OF STENTED PHANTOM SHOWING STENT

3.3   CFD MESH GENERATION

The ultimate objective of the development of these models was the production of models that can be utilised for CFD analysis. Once the stented and non-stented models were developed, both underwent post-processing in order to be suitable for deployment in the CFD pipeline. The nature and extent of this processing varied between both models due to the disparity in internal geometries. The CFD analysis for these post-processed meshes were deployed through the National Computational Infrastructure (NCI).

Once the reconstructed models have been obtained, they need to be post processed for CFD analysis. This involved isolating the model to just leave the inner lumen and smoothing the model to ensure that it resembled the inner lumen of a blood vessel and generating a CFD Mesh as an input to ANSYS.

M Marriott, Undergraduate Thesis

3.3.1 NON-STENTED CFD MESH GENERATION

Generating the Non-Stented Phantom reconstructed model was carried out first. The outer wall of the non-stented model was isolated to the inner lumen. From there, the vessel was cropped to save computational time.

VMTK functions were then used to generate the CFD mesh, this involved tetrahedralizing the mesh, defining the inlets and outlets, computing the centrelines and outputting the mesh in a format that is accepted by the ANSYS setup tool.
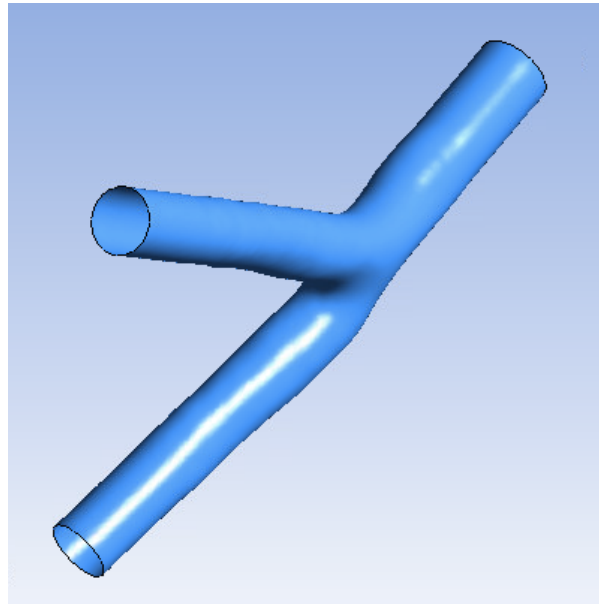

FIGURE 18 - CFD MESH FOR NON-STENTED MODEL

3.3.2 STENTED CFD MESH GENERATION

The addition of the stent added significant complexity to the internal geometry. Two different approaches were explored as a means of producing a CFD mesh that would be acceptable for analysis. The generation technique carried out through VMTK was concluded as insufficient as the functions could not compute a mesh with the complexity of both the stent and vessel simultaneously. Therefore, ANSYS meshing was used to generate the mesh as it had the capability of generating a mesh accounting for the obstruction due to the stent.

M Marriott, Undergraduate Thesis

The vessel model was imported into Meshlab where it was downsampled using the Unified Mesh Resampling application, which allows a simplification of the model, after which a Taubin Smooth was performed to smooth the surface of the vessel. The stent was also downsampled in VMTK to allow for lesser processing time and then the same steps were executed on the stent also. This downsampling and smoothing was needed to ensure the input was accepted by the ANSYS, as rough surfaces will cause a failure in meshing.

Once the pre-processing was carried out, both the stent and vessel STLs were imported into ANSYS to generate a CFD Mesh. Figures 19 and 20 show the input to CFD for the stented model; the surface of the vessel clearly shows the imprint of the stent on the surface and the stent geometry is present, obstructing the fluid flow.
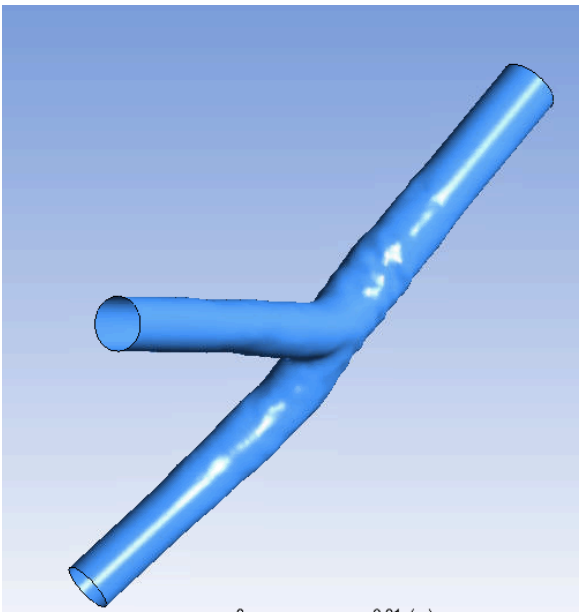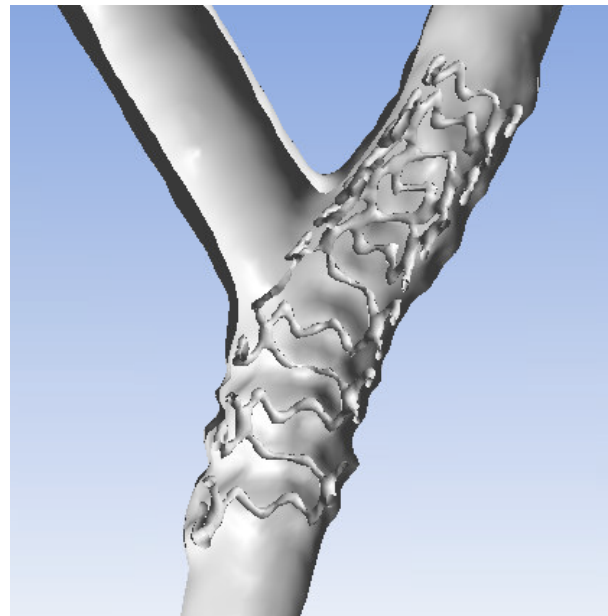

FIGURE 19 - CFD MESH STENTED MODEL

FIGURE 20 - CFD MESH FOR STENTED MODEL SHOWING INTERNAL STENT GEOMETRY

The ANSYS workflow generated was then uploaded and run through NCI to produce a CFD solution. This solution was then post-processed to produce plots for the velocity, WSS and TAWSS so the final output for both can be compared and validated.

25

M Marriott, Undergraduate Thesis

4. RESULTS AND DISCUSSION

The above methodology produced two distinct modelling techniques, each vastly different in their final output. On evaluation of each method, it was found that the micro-CT reconstructed model was superior in terms of representing the geometry of the stented phantom and the current modelling approach was updated and is summarised in figure 21. Despite this, there are still shortcomings and errors identified with this approach that must be considered when viewing the final output.
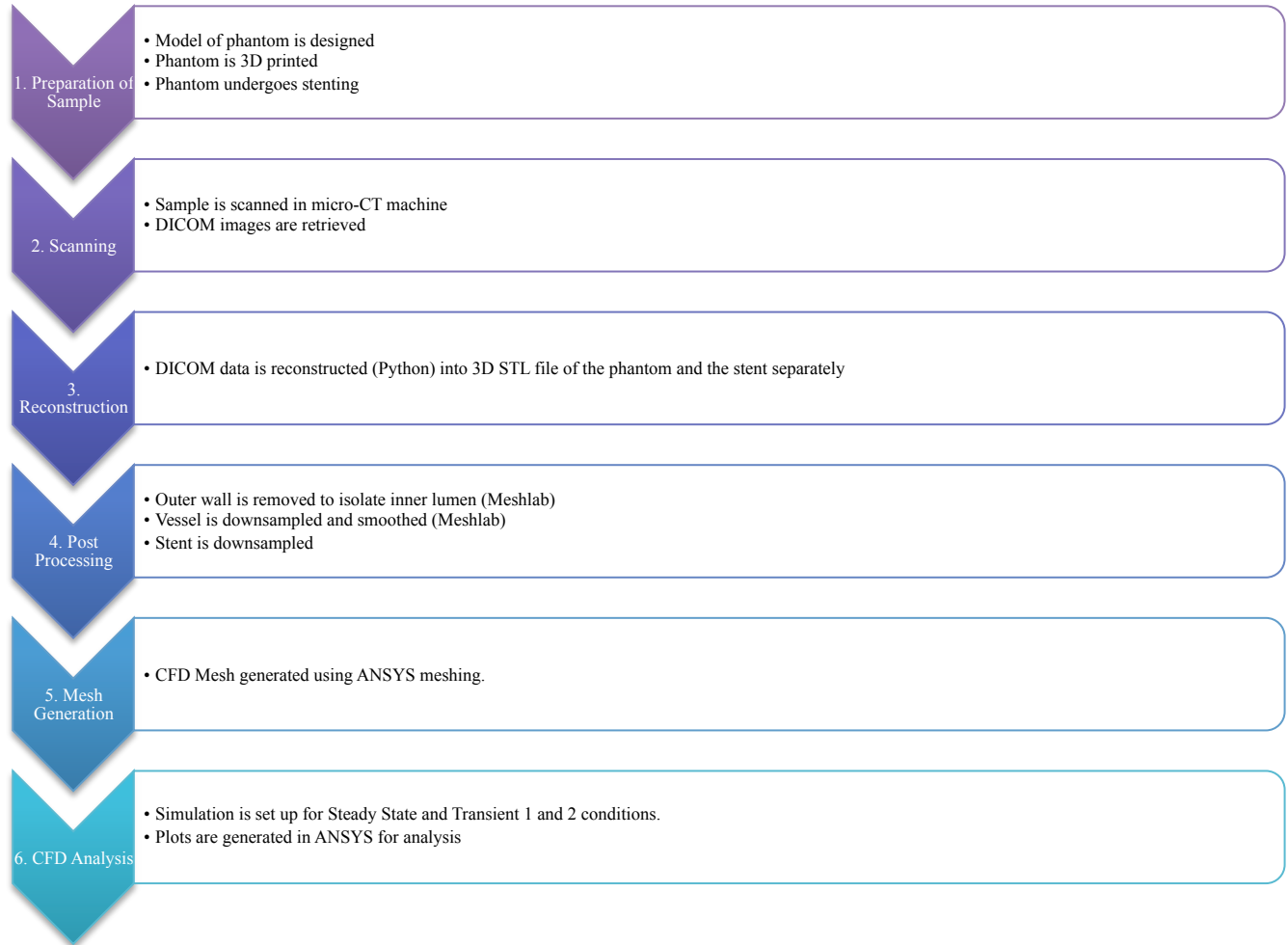

1. Preparation of Sample
- Model of phantom is designed
- Phantom is 3D printed
- Phantom undergoes stenting

2. Scanning
- Sample is scanned in micro-CT machine
- DICOM images are retrieved

3. Reconstruction
- DICOM data is reconstructed (Python) into 3D STL file of the phantom and the stent separately

4. Post Processing
- Outer wall is removed to isolate inner lumen (Meshlab)
- Vessel is downsampled and smoothed (Meshlab)
- Stent is downsampled

5. Mesh Generation
- CFD Mesh generated using ANSYS meshing.

6. CFD Analysis
- Simulation is set up for Steady State and Transient 1 and 2 conditions.
- Plots are generated in ANSYS for analysis

FIGURE 21 - CURRENT MODELLING AND DEPLOYMENT PROCESS FOR STENTED PHANTOMS

M Marriott, Undergraduate Thesis

4.1 ALIGNMENT

The revised alignment method resulted in producing an identical output to Bakiris' work in 2018, but allowed for a more reliable delivery of these results. The improvements to Matlab alignment resulted in a more consistent output subject to little human error when executed. X-ray images of the phantom were obtained before and after stenting when the micro-CT images were captured. This was valuable in that it provided a means of visual comparison between the model produced through alignment and the appearance of the inner lumen of the stented phantom.

From a simple visual comparison, it is clear that the significant bending and deforming of the inner lumen produced by the alignment method is significantly greater than that is visible in the changing of the Stented Phantom. It appears from a purely visible standpoint that the alignment method is rather drastic in its manipulation of the inner lumen.

It is also significant that the alignment method does not incorporate the impression of the stent or the stent itself into the final output, which would result in a CFD model that does not account for the obstruction of the stent itself, which would cause significant discrepancies between the simulated and actual fluid behaviour.

It was concluded that the micro-CT reconstructed image demonstrates a greater extent of accuracy than that produced by the revised alignment method. Therefore, the desired methodology was concluded to be that of the micro-CT.
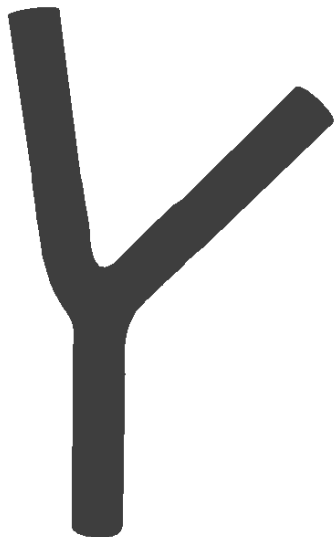
M Marriott, Undergraduate Thesis

FIGURE 22 - INNER LUMEN OF VESSEL PRIOR TO ALIGNMENT

FIGURE 23 – ALIGNMENT OUTPUT
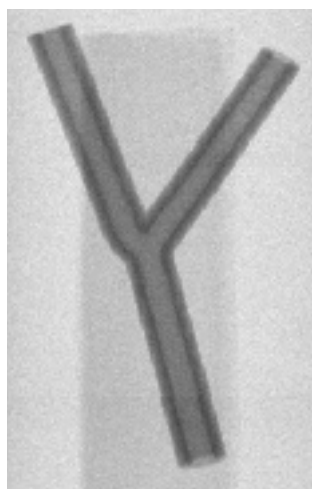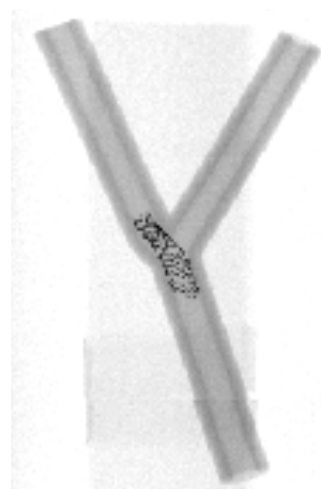

FIGURE 24 - X-RAY IMAGE OF PHANTOM PRE-STENTING

FIGURE 25 - X-RAY IMAGE OF PHANTOM POST-STENTING

M Marriott, Undergraduate Thesis

4.2 MICRO-CT RECONSTRUCTION

Despite overcoming the shortcomings previously identified by Bakiris involving the presence of the metal stent, there are limitations to the model produced by the micro-CT reconstruction method. The result shows malapposition of the stent; a gap between the vessel wall and the stent. The presence of this could be attributed to either a deployment issue or an issue with the reconstruction. Additionally, the DICOMs produced from the scan show presence of artifacts due to the luminosity of the metallic stent. As a result, the VTK morphological functions used to extract the two separate objects, the vessel and the stent, could be attributing features to either that are not indicative of the true geometry. The surface of the vessel from the reconstruction shows deformation to a greater extent than expected, which could be the attributed to medical imaging defects.

Aside from the potential errors through imaging and reconstruction, the methods used to generate the CFD mesh required smoothing and downsampling in order to execute the mesh generation. Because of this, there is a potential loss of geometry of the final mesh.

4.2.1 MALAPPOSED STENT

As evident in figure 20 showing the stented region of the CFD input, there is a visible gap between the stent and the wall of the vessel in the branch. The presence of this gap in an actual patient would cause immediate complications, increasing the risk of stent thrombosis [18]. This malapposition could be due to the actual implantation; as the surgical procedure of implanting the stent is vastly different to the implantation in an actual patient. Because of this, there could have been issues with deployment.

From figures 26 through 28, showing two DICOM slices of the stented area as well as an X-ray image of the stented phantom, it can be concluded with confidence that the malapposition is consistent from the initial micro-CT scan to the reconstructed model. Therefore, it is unlikely that any malapposition viewed is a result of image artifacts or errors in the reconstruction. When viewing the DICOM slices of the vessel, there are clear misalignments between the vessel inner lumen and the stent. It is possible that errors in the reconstruction techniques could cause some misalignment, but the presence of this phenomenon in both the micro-CT images and the reconstructed model indicates that the integrity of these images was translated to the final model. This is further validated by the X-ray images captured prior to the micro-CT scan (figure 28), in which there is clear malapposition present.
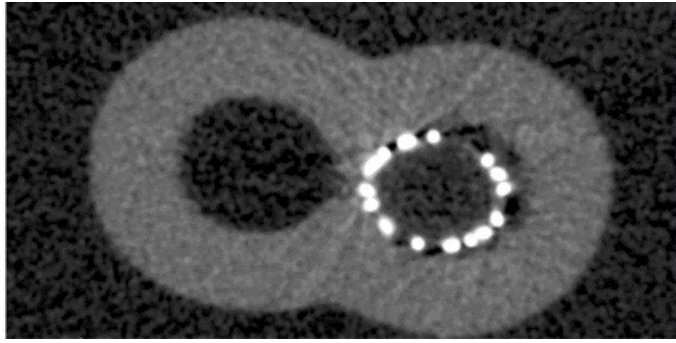
M Marriott, Undergraduate Thesis

FIGURE 26 - MICRO-CT IMAGE OF STENTED VESSEL SHOWING MALAPPOSITION (1)
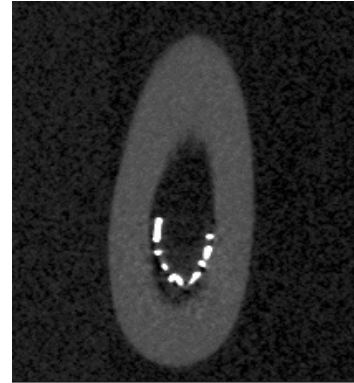

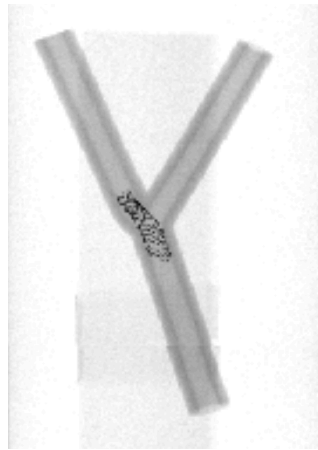**FIGURE 27 - MICRO-CT IMAGE OF STENTED VESSEL SHOWING MALAPPOSITION (2)**

FIGURE 28 - X-RAY IMAGE OF STENTED PHANTOM

4.2.2 PRESENCE OF ARTIFACTS

The micro-CT images show a slight presence of artifacts, identified by the slight blooming and streaking of the highly luminous stent in figures 26 and 27. Despite these being small and not completely obstructing the structure of the vessel; the presence of them can add error to the image as they are identifying objects that are not present on the phantom or stent themselves. This could lead to potential complications; as discussed in section 2.2, the output for the stented reconstructed model required additional smoothing prior to the CFD mesh generation, due to an increased roughness around the stented area. This roughness can be attributed to medical imaging artifacts. Issues arise here as excessive

M Marriott, Undergraduate Thesis

smoothing of the model can result in loss of geometry, resulting is a less accurate representation of the phantom.

4.2.3 VESSEL WALL INDENTATION

Another area of concern when viewing the output of the reconstruction for the stented phantom was the degree of indentation the stent caused on the vessel wall. While this could be expected to take place, the indentation visible in figures 19 and 20 is more significant than expected in the vessel wall prior to the bifurcation. To evaluate if the stent is embedded in the vessel wall, The individual DICOMs for three corresponding locations along the vessel to compare the stents impact on the inner lumen. These images are shown in figures 29 through 34.

M Marriott, Undergraduate Thesis
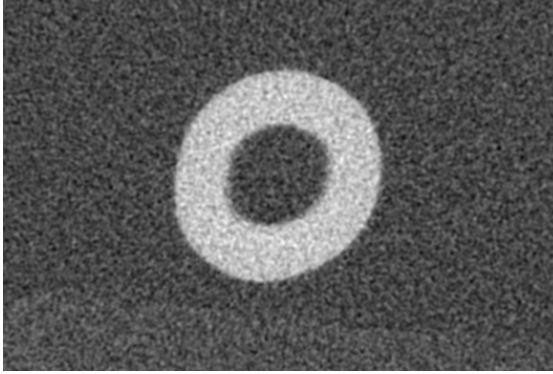
FIGURE 29 - NON-STENTED DICOM IMAGE (1)
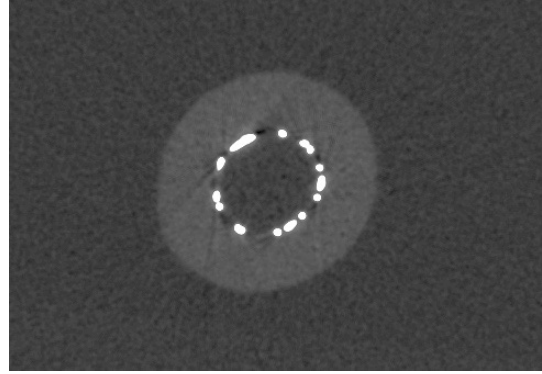
FIGURE 30 - STENTED DICOM IMAGE (1)
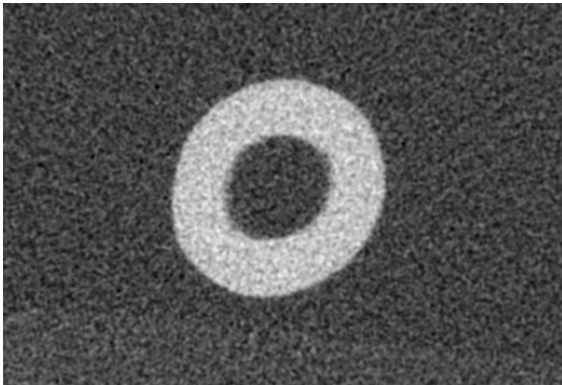
FIGURE 31 - NON-STENTED DICOM IMAGE (2)
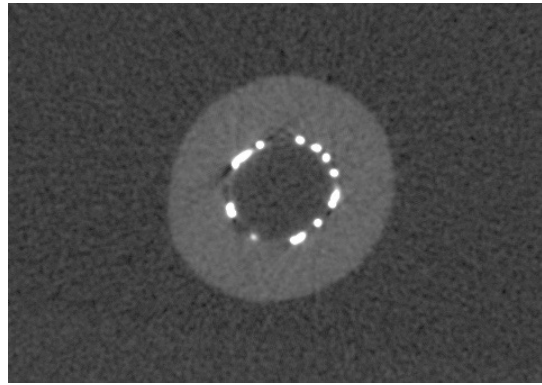
FIGURE 32 - STENTED DICOM IMAGE (2)
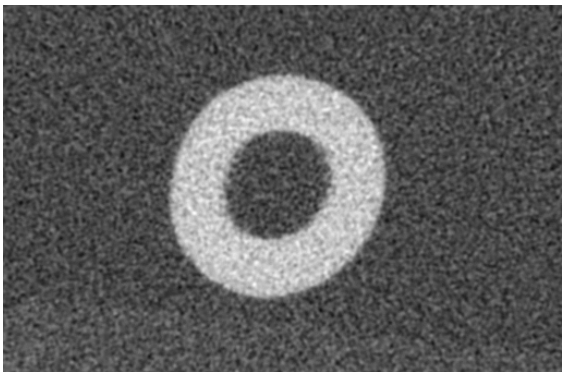
FIGURE 33 - NON-STENTED DICOM IMAGE (3)
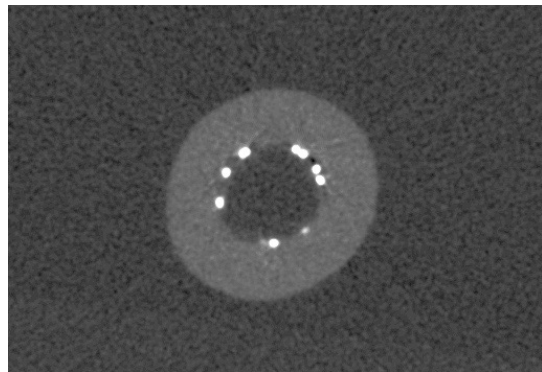

FIGURE 34 – STENTED DICOM IMAGE (3)

32

M Marriott, Undergraduate Thesis

From visual inspection, the stent struts appear in all three instances to be embedded in the inner lumen rather than situated at the surface, would explain the significant impression left by the stent. A cause of this could be the material of the phantom being too soft and allowing for significant indenting of the stent. In addition, this could be attributed to the stent being implanted with more force than typically applied. As discussed previously, the blooming artifacts due to the luminosity of the metal could be increasing the appearance of the stent captured in the scan. This should be considered when discussing and analysing the CFD results.

4.2.4 SMOOTHING AND SIMPLIFICATION OF THE FINAL MESH

In order for the geometry generated from the reconstruction to be accepted by the ANSYS meshing software, it needs to be smooth enough for the mesh to be generated. The reconstructed stent and vessel files were underwent smoothing in order to allow ANSYS to accept the geometry. This should be considered when viewing the final results, as there is a potential loss of geometry captured in the final mesh. Due to the limitations of the software, this is a tradeoff that must occur to produce a workable model and is a significant limitation in producing an accurate final model.

4.2.5 CFD RESULTS VERIFICATION

In order to verify the modelling approach and conclude its accuracy in representing a stented phantom, there is a need to quantify the extent to which the ideal geometry is achieved. A clear means of determining the validity of the output is to analyse the output of the CFD analysis, using the fluid behaviour through the velocity profiles and the shear stress compared to literature in order to determine the feasibility of this approach.

The two models of the surface for the stented and non-stented vessels were used to generate CFD meshes and were setup for CFD analysis. The results from each were compared using velocity, WSS and TAWSS as means for comparison. It was found that the behaviour of the stented model in terms of these metrics aligns with the expected behaviour and therefore provides verification for the model produced.

4.2.5.1 VELOCITY

Visualising the streamlines through both models will provide an overall view of how the fluid moves throughout the vessels. In order to validate the model using the streamlines, we would expect the obstruction due to the stent to be visable through the behaviour of the streamlines. Figures 35 and 36

M Marriott, Undergraduate Thesis

show the streamlines for the stented and non-stented models respectively, with the stent outline visable. Figures 37 and 38 show the same streamlines but focus on the stented region and provide a closer look at the streamline behaviour in this region. 40 streamlines were seeded at each inlet of the models to demonstrate the fluid behaviour through each model.

The non-stented model in figure 35 shows a consistent velocity profile leading to the bifurcation, after which this profile is disrupted as the flow is diverted to different branches. The stented model shows this same behaviour in figure 36, however the stented branch (bottom branch) shows narrowing of the passage the streamlines flow through.

Comparing figures 37 and 38, there is a clear narrowing of the streamlines approaching the bifurcation on the stented model that is not present on the non-stented model, indicating the stent is disrupting the flow in this area. This is consistent with the behaviour that would be expected with the stent in place, as the disruption to the wall of the stent results in disruption to the streamlines at the boundary layer. In addition, the velocity at this point of narrowing shows an increase, which aligns with the expected behaviour of a narrowing fluid region.

A similar narrowing can be seen on the stented branch post-junction (bottom branch), where the malapposition has deviated the streamlines. There is also a disruption to the streamlines visible in the non-stented branch (top) due to the struts obstructing the bloodflow at the junction.

From this flow observation, it can be concluded that the stent is manipulating the flow in an expected manner. A closer look into the velocity distribution throughout this stented area for both models will provide further insight into the effect of the stent.
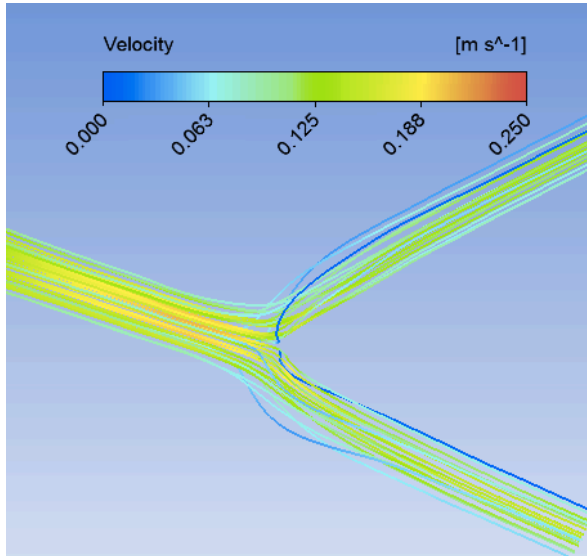
M Marriott, Undergraduate Thesis

FIGURE 35 - STREAMLINES NON-STENTED MODEL
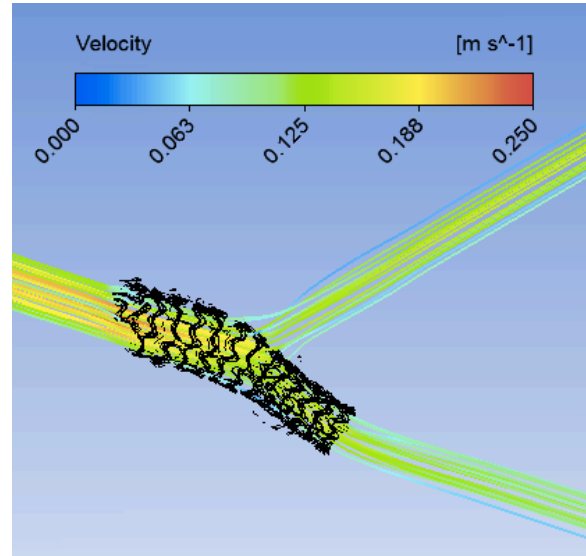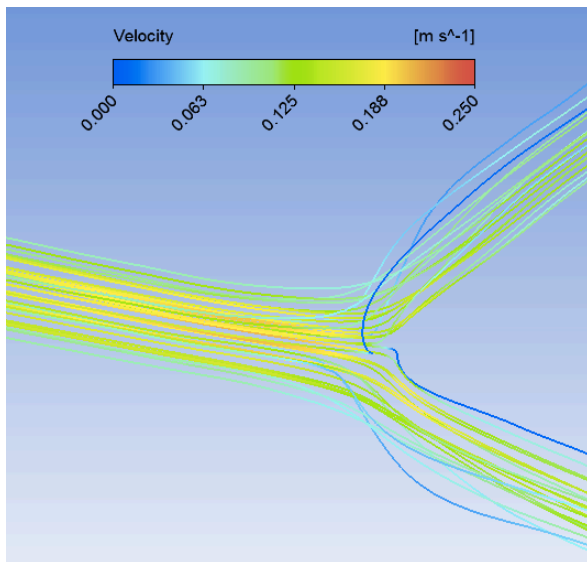

FIGURE 36 - STREAMLINES STENTED MODEL

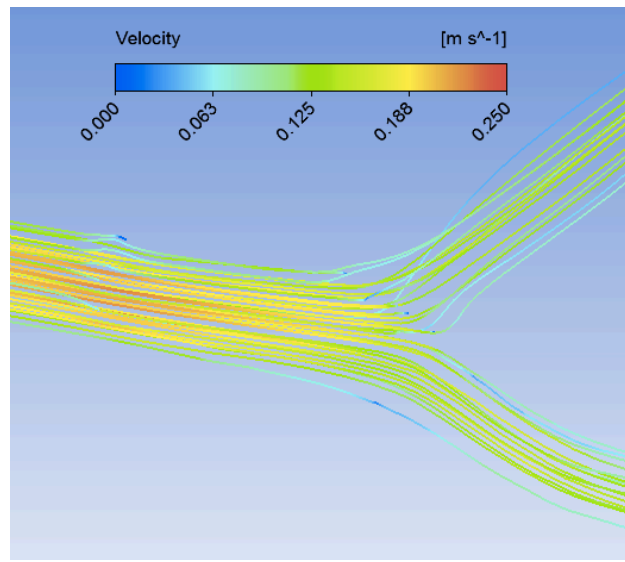**FIGURE 37 – STREAMLINES OF NON-STENTED MODEL (STENTED AREA)**

FIGURE 38 - STREAMLINES OF STENTED MODEL (STENTED AREA)

M Marriott, Undergraduate Thesis

The velocity profile around the stented area can give insight into whether or not the behaviour is reflecting that of a stented phantom. Figures 39 and 40 show the velocity behaviour in the non-stented and stented models respectively.

The non-stented model reflects the expected behaviour. At the junction there is a decrease in velocity due to the bifurcation, after which the velocity is highest towards the inside walls before it gradually develops.

The stented model reflects the behaviour expected from literature. At the location of the stent struts, there is an area of low velocity surrounding the strut. As discussed in section 2.4.1.1, the irregularity caused by the introduction of a stent will cause the outermost regions of fluid to decrease in velocity due to recirculation. The presence of the struts results in an increase in the low velocity boundary layer as the disruption to the flow causes areas of turbulence and recirculation around the struts. This behaviour is visible at all strut locations visable before and after the bifurcation. The blockage of the bloodflow due to the stent on the non-stented branch decreases the velocity entering this branch.

Although this behaviour reflects what is expected, for a vessel wall with less indentation there would be a greater extent of disruption to the velocity caused by the stent, as the stent obstructs the flow to a greater extent when it is not embedded in the wall.
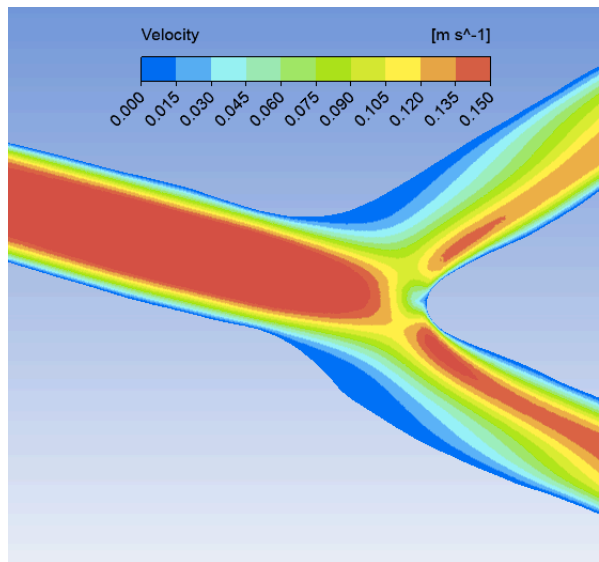

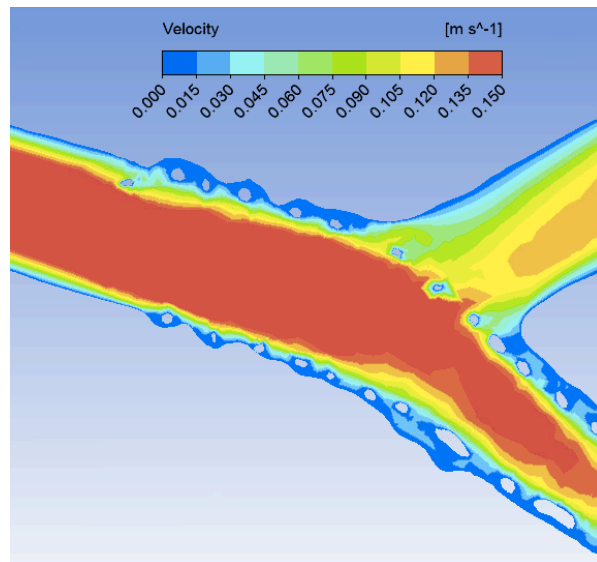**FIGURE 39 - VELOCITY CROSS-SECTON OF NON-STENTED MODEL**

FIGURE 40 - VELOCITY CROSS-SECTION OF STENTED MODEL

M Marriott, Undergraduate Thesis

The Wall Shear Stress (WSS) and Time Averaged Wall Shear Stress (TAWSS) show distinct behaviour in stented vessels; there will be distict drops in WSS and TAWSS where the stent is present, and this WSS and TAWSS will increase once the stented area is passed.

Figures 41 and 42 show the WSS distribution on the wall of the vessel for both models. The non-stented model shows alignment with the literature, as a similar behaviour is captured as discussed in section 2.4.1.2. As for the stented model, there is a clear drop in WSS at the stent location. This is consistent with the velocity observed, as the changes introduced to the velocity result in lower WSS.
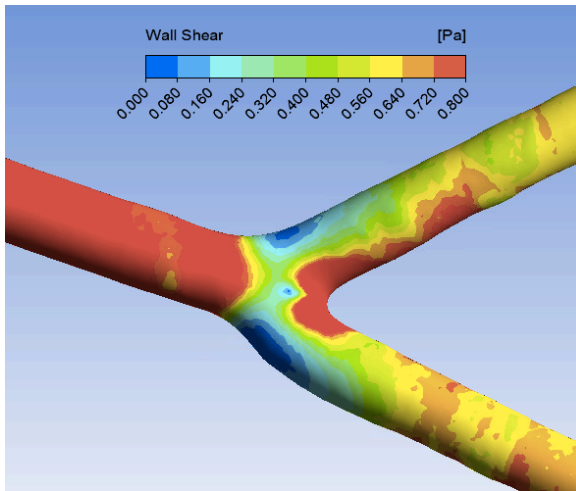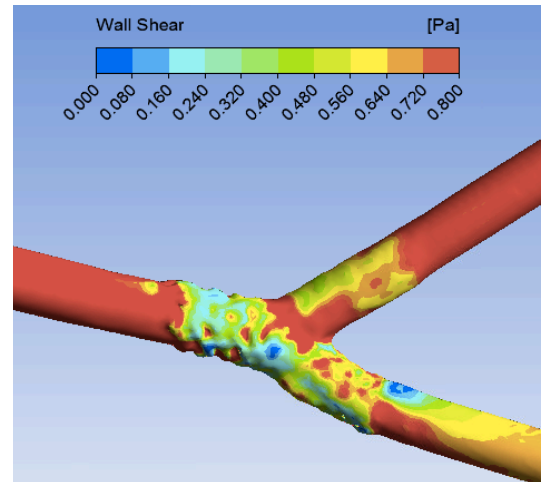

FIGURE 41 - WSS NON-STENTED MODEL

FIGURE 42 - WSS STENTED MODEL

A closer perspective of the stented region of the WSS and TAWSS for the models can be seen in figures 43 through 46.

Comparing the region of both models approaching the bifurcation, the non-stented models show consistent WSS and TAWSS values above 0.8Pa. There is a slight drop shown approaching the junction, this could be attributed to a lack of smoothness in the geometry in this section, either due to the actual surface of the phantom or due to error introduced during the reconstruction, post-processing or mesh generation phases.

Once approaching the bifurcation, low WSS and TAWSS is observed in the stent regions, fluctuating in accordance to the strut locations.
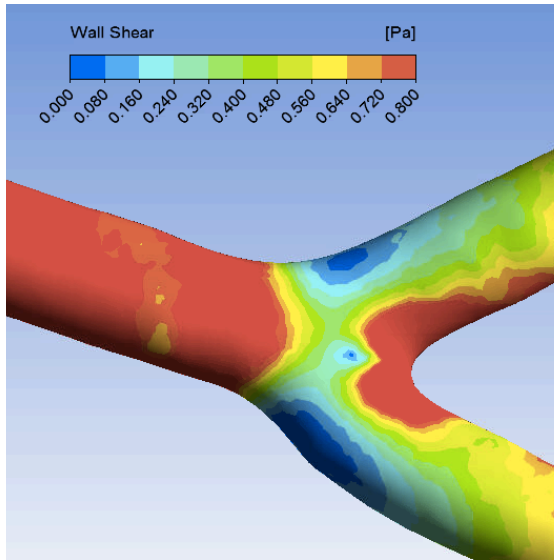
M Marriott, Undergraduate Thesis

FIGURE 43 - WSS NON-STENTED MODEL
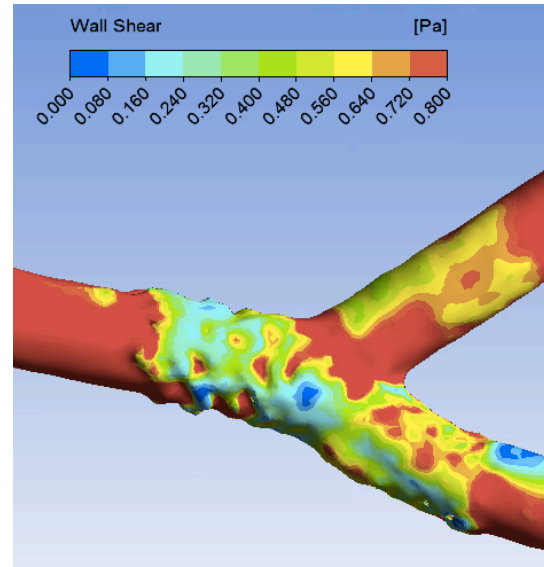

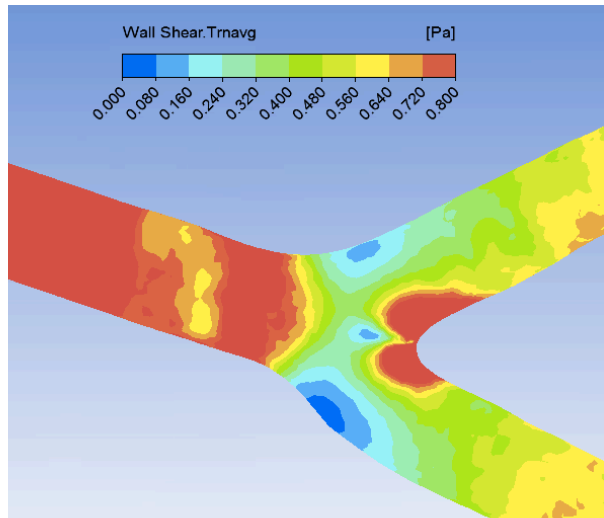**FIGURE 44 - WSS STENTED MODEL**

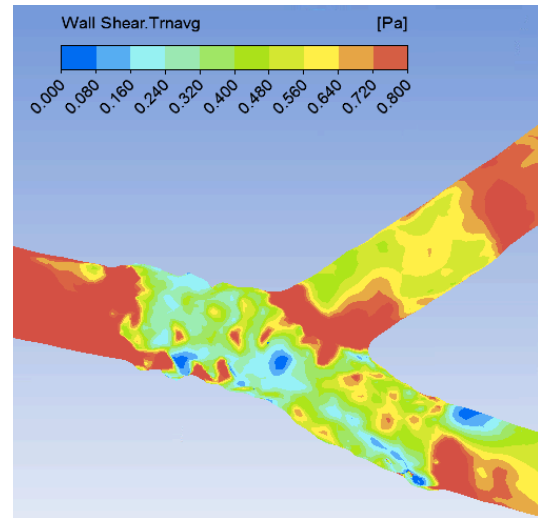**FIGURE 45 - TAWSS NON-STENTED MODEL**

FIGURE 46 - TAWSS STENTED MODEL

Figures 47 and 48 show a cross-section of the WSS and TAWSS for the stented model. This plot shows relatively higher WSS and TAWSS on the stent compared to the wall, exemplified by the red sections of

38

M Marriott, Undergraduate Thesis

the stent. The malapposed region, after the bifurcation where there is a clear separation between the vessel wall and the stent, shows high WSS and TAWSS values, as it is obstructing areas of high fluid velocity and it therefore subject to a greater instance of shear stress.
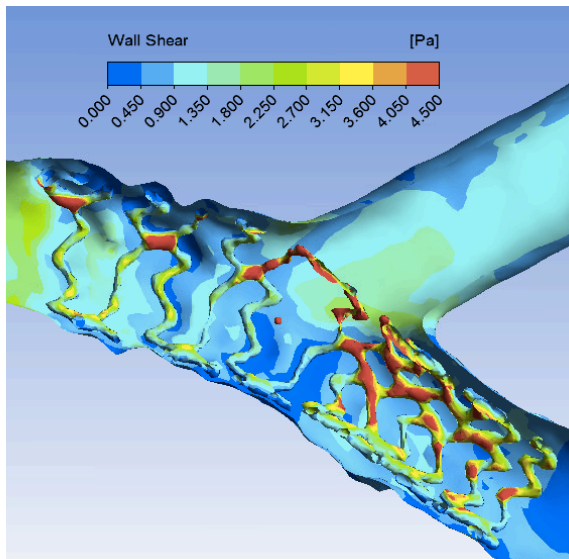

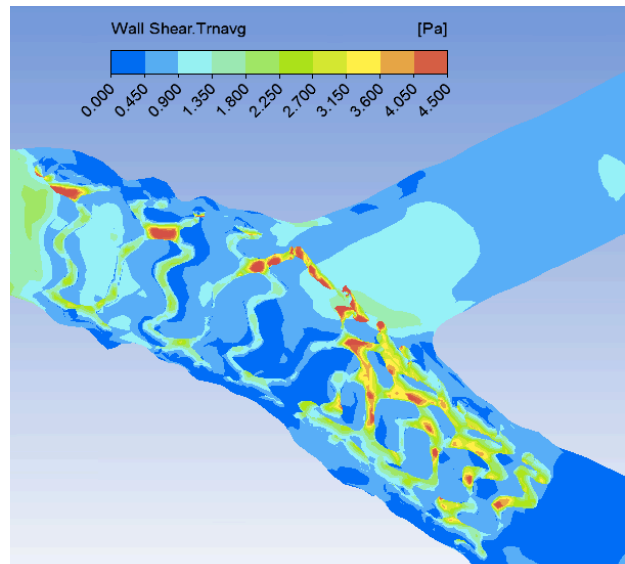**FIGURE 47 – CROSS-SECTION OF WSS FOR NON-STENTED MODELS**

FIGURE 48 – CROSS-SECTION OF TAWSS FOR STENTED MODEL

From analysis of the CFD output, it can be concluded with confidence that the results exemplify the behaviour of a stented coronary artery. It can be concluded that the geometry and fluid characteristics align with the expected behaviour, however it is difficult to conclude slight variations in geometry due to oversimplification and smoothing of the geometry in the post-processing phase as well as inconsistencies in geometry captured due to medical imaging defects. As this technique has only been examined on one sample, further iterations could provide further validation and uncover any inconsistencies present in the current method.

M Marriott, Undergraduate Thesis

5. FUTURE WORK

In terms of further development, there is significant potential for the application of this technique to investigate the phenomenon of stented arteries and their failure modes. In addition to this, however, there is a need for further improvement and validation of the process used, through further replication.

This process has been carried out in its entirety on one sample, pre- and post-stenting, further understanding of the accuracy of this approach requires investigation into different vessel geometries and stent locations to ensure that the method is widely applicable. This would provide further validation of the technique as well as further optimisation. Additionally, alternative meshing techniques could be explored beyond that trialled in this body of work; smoothing and downsampling was needed to prepare the geometry for meshing, which could have resulted in loss of key geometry and introduced further inaccuracy to the results captured. Exploring alternatives to meshing could prove helpful in improving mesh quality for the final output. More optimisation could also be focused around imaging techniques, stenting techniques and material selection for phantoms.

This process could be valuable in the application of diseased models. The underlying cause of Coronary Artery Disease is atherosclerosis, in which there is a buildup of plaque inside the artery wall affecting the blood flow [36]. Using 3D printing technology it is possible to replicate the geometry and the material properties of the plaque in diseased arteries, which can be subsequently stented and modelled to analyse the fluid behaviour and gain further understanding of the failure modes in vessels with different disease.

6. CONCLUSION

Investigating the use of alignment methods and micro-CT reconstruction have resulted in the development of a process for modelling stented phantoms. The current method deviated from the incorporating alignment by reintroducing micro-CT reconstruction as a method, resulting in a final model that resembles the stented phantom to a greater extent.

There is a need to further validate this process through further testing and trialling different post-processing and meshing techniques as well as further insight into the material properties and stenting techniques employed. However, this process has potential for accurately capturing the internal geometry of stented phantoms and ultimately aiding in the production of accurate CFD models of stented arteries to help analyse and understand the failure modes of stents in patients.

M Marriott, Undergraduate Thesis

7. REFERENCES

[1] Iqbal, J., Gunn, J. and Serruys, P.W., 2013. Coronary stents: historical development, current status and future directions. Br Med Bull, 106(1), pp.193-211.

[2] Medline Plus. Angioplasty and stent placement – heart, 2019. Available at https://medlineplus.gov/ency/article/007473.htm

[3] Beier, S., Ormiston, J., Webster, M., Cater, J., Norris, S., Medrano-Gracia, P., Young, A. and Cowan, B., 2016. Hemodynamics in idealized stented coronary arteries: important stent design considerations.

[4] Van der Heiden, K., Gijsen, F.J., Narracott, A., Hsiao, S., Halliday, I., Gunn, J., Wentzel, J.J. and Evans, P.C., 2013. The effects of stenting on shear stress: relevance to endothelial injury and repair. Cardiovascular research, 99(2), pp.269-275.

[5] Bakiris, V, 2018, Stented Artery Computational Modelling, Honours Thesis, University of New South Wales, Sydney

[6] Liao, R., Chen, S.Y.J., Messenger, J.C., Groves, B.M., Burchenal, J.E.B. and Carroll, J.D., 2002. Four dimensional analysis of cyclic changes in coronary artery shape. Catheterization and cardiovascular interventions, 55(3), pp.344-354.

[7] Chen, E.C., McLeod, A.J., Baxter, J.S. and Peters, T.M., 2015. Registration of 3D shapes under anisotropic scaling. International journal of computer assisted radiology and surgery, 10(6), pp.867-878

[8] Rohlf, F.J., 1990, May. Rotational fit (Procrustes) methods. In Proceedings of the Michigan morphometrics workshop (No. 2, pp. 227-236). Ann Arbor: University of Michigan Museum of Zoology.

[9] Paláncz, B., Zaletnyik, P., Awange, J.L. and Heck, B., 2010. Extension of the ABC-Procrustes algorithm for 3D affine coordinate transformation. Earth, planets and space, 62(11), p.857.

42

[10] Magnusson, M., 2009. The three-dimensional normal-distributions transform: an efficient representation for registration, surface analysis, and loop detection (Doctoral dissertation, Örebro universitet).

[11] Farnia, P., Ahmadian, A., Sedighpoor, M., Khoshnevisan, A. and Mansoory, M.S., 2012. On the performance of improved ICP algorithms for registration of intra-ultrasound with pre-MR images; a phantom study. In 2012 Annual International Conference of the IEEE Engineering in Medicine and Biology Society (pp. 4390-4393). IEEE.

[12] Li, H., Kim, E., Huang, X. and He, L., 2010, June. Object matching with a locally affine-invariant constraint. In 2010 IEEE Computer Society Conference on Computer Vision and Pattern Recognition (pp. 1641-1648). IEEE.

[13] Australian Institute of Health and Welfare. Australia's Health 2016. Technical Report Cat. no. AUS 199, Australias health series no. 15, Canberra, 2016.

[14] Alfonso, F., Zueco, J., Cequier, A., Mantilla, R., Bethencourt, A., López-Minguez, J.R., Angel, J., Augé, J.M., Gómez-Recio, M., Morís, C. and Seabra-Gomes, R., 2003. A randomized comparison ofrepeat stenting with balloon angioplasty in patients with in-stent restenosis. Journal of the American College of Cardiology, 42(5), pp.796-805.

[15] Australian Institute of Health and Welfare. Australia's Health 2016. Technical Report Cat. no. AUS 199, Australias health series no. 15, Canberra, 2016.

 [16] Brook, O.R., Gourtsoyianni, S., Brook, A., Mahadevan, A., Wilcox, C. and Raptopoulos, V., 2012. Spectral CT with metal artifacts reduction software for improvement of tumor visibility in the vicinity of gold fiducial markers. Radiology, 26 (3), pp.696-705.

[17] Hegazy, M.A., Cho, M.H. and Lee, S.Y., 2016. A metal artifact reduction method for a dental CT based on adaptive local thresholding and prior image generation. Biomedical engineering online, 15(1), p.119.

[18] Tanigawa, J., Barlis, P., Dimopoulos, K., Dalby, M., Moore, P. and Di Mario, C., 2009. The influence of strut thickness and cell design on immediate apposition of drug-eluting stents assessed by

M Marriott, Undergraduate Thesis

optical coherence tomography. International journal of cardiology, 134(2), pp.180-188.

[19] www.cvphysiology.com. (n.d.). CV Physiology | Laminar Flow. [online] Available at: https://www.cvphysiology.com/Hemodynamics/H006#:~:text=It%20is%20characterized%20by%20conce ntric [Accessed 25 Jul. 2020].

[20] Shaaban, A.M. and Duerinckx, A.J., 2000. Wall shear stress and early atherosclerosis: a review. American Journal of Roentgenology, 174(6), pp.1657-1665.

[21] Papaioannou, T.G. and Stefanadis, C., 2005. Vascular wall shear stress: basic principles and methods. Hellenic J Cardiol, 46(1), pp.9-15.

[22] Katritsis, D., Kaiktsis, L., Chaniotis, A., Pantos, J., Efstathopoulos, E.P. and Marmarelis, V., 2007. Wall shear stress: theoretical considerations and methods of measurement. Progress in cardiovascular diseases, 49(5), pp.307-329.

[23] Chiastra, C., Migliavacca, F., Martínez, M.Á. and Malvè, M., 2014. On the necessity of modelling fluid–structure interaction for stented coronary arteries. Journal of the mechanical behavior of biomedical materials, 34, pp.217-230.

[24] Martin DM, et al. Computational fluid dynamics analysis of balloon-expandable coronary stents: Influence of stent and vessel deformation. Med Eng Phys (2014), http://dx.doi.org/10.1016/j.medengphy.2014.05.011

[25] Gundert, T.J., Marsden, A.L., Yang, W. and LaDisa, J.F., 2012. Optimization of cardiovascular stent design using computational fluid dynamics. Journal of biomechanical engineering, 134(1).

[26] S. Morlacchi and F. Migliavacca. Modeling Stented Coronary Arteries: Where We are, Where to Go. Annals of Biomedical Engineering, 41(7):1428–1444, 2013.

[27] Benard, N., Coisne, D., Donal, E. and Perrault, R., 2003. Experimental study of laminar blood flow through an artery treated by a stent implantation: characterisation of intra-stent wall shear stress. Journal of biomechanics, 36(7), pp.991-998.

[28] Sera, T., Yagi, N. and Uesugi, K., 2004, September. Three-dimensional visualization of intact mouse lung by synchrotron radiation CT. In The 26th Annual International

M Marriott, Undergraduate Thesis

[29] Wang, K., Ho, C.C., Zhang, C. and Wang, B., 2017. A review on the 3D printing of functional structures for medical phantoms and regenerated tissue and organ applications. Engineering, 3(5), pp.653-662.

[30] Filippou, V. and Tsoumpas, C., 2018. Recent advances on the development of phantoms using 3D printing for imaging with CT, MRI, PET, SPECT, and ultrasound. Medical physics, 45(9), pp.e740-e760.

[31] Micro Photonics. (2018). What is Micro-CT? An Introduction. [online] Available at: https://www.microphotonics.com/what-is-micro-ct-an-introduction/.

[32] Barrett, J.F. and Keat, N., 2004. Artifacts in CT: recognition and avoidance. Radiographics, 24(6), pp.1679-1691.

[33] Onishi, H., Hori, M., Ota, T., Nakamoto, A., Osuga, K., Tatsumi, M., Fukui, H., Tsukagoshi, S., Uranishi, A., Saito, Y. and Taniguchi, A., 2018. Phantom study of in-stent restenosis at high-spatial-resolution CT. Radiology, 289(1), pp.255-260.

[34] Boas, F.E. and Fleischmann, D., 2012. CT artifacts: causes and reduction techniques. Imaging in medicine, 4(2), pp.229-240.

[35] Rikhtegar, F., Wyss, C., Stok, K.S., Poulikakos, D., Müller, R. and Kurtcuoglu, V., 2014. Hemodynamics in coronary arteries with overlapping stents. Journal of biomechanics, 47(2), pp.505-511.

[36] "What is coronary heart disease?," Heart Foundation, [Online]. https://www.heartfoundation.org.au/your-heart/heart-conditions/what-is-coronary-heart-disease. [March 2019].

[37] Hammes, M., Boghosian, M., Cassel, K., Watson, S., Funaki, B., Doshi, T., Mahmoudzadeh Akherat, S.J., Hines, J. and Coe, F., 2016. Increased inlet blood flow velocity predicts low wall shear stress in the cephalic arch of patients with brachiocephalic fistula access. PloS one, 11(4), p.e0152873.

[38] Pinto, S.I.S. and Campos, J.B.L.M., 2016. Numerical study of wall shear stress-based descriptors in the human left coronary artery. Computer methods in biomechanics and biomedical engineering, 19(13), pp.1443-1455.
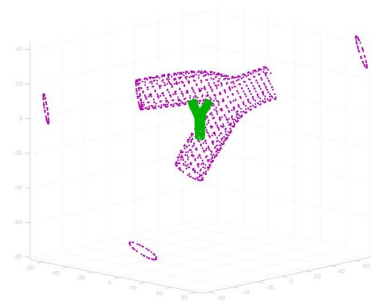
M Marriott, Undergraduate Thesis

8. Appendices

Appendix A - Limitations to NDT Alignment Implementation
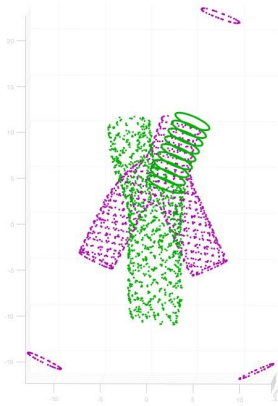
Appendix A.1
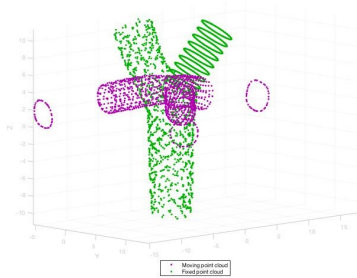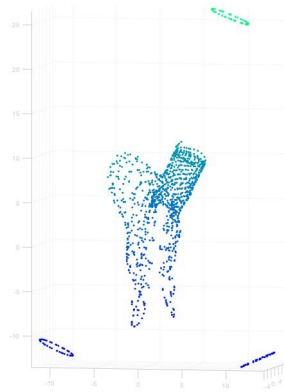

Initial Inputs with Perpendicular Vessel

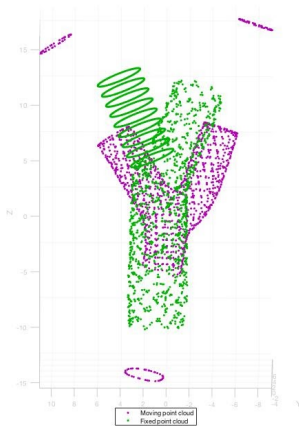Post-Scaled Vessel and Stent with Perpendicular Vessel after NDT and ICP Alignment

i

Appendix A.2
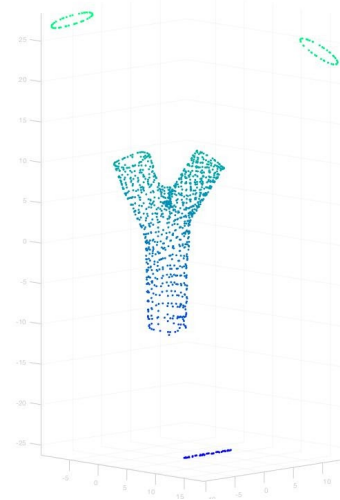

Initial Inputs with Perpendicular Vessel

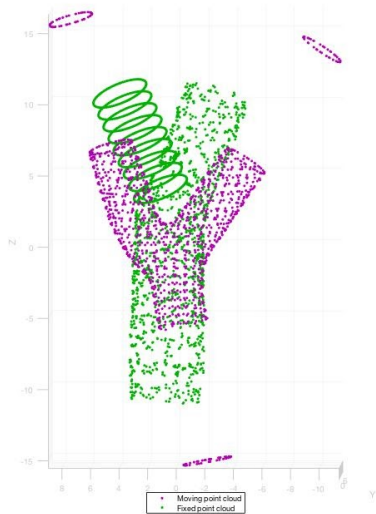

Final Output with Upside Down Vessel Input

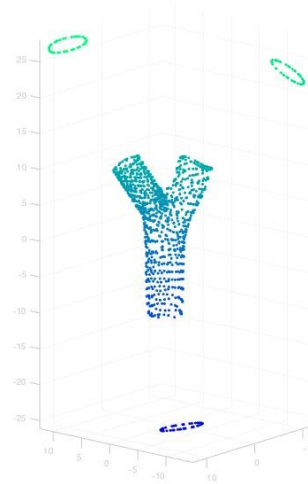**Appendix A.3**

Input Vessel and Stent correctly aligned

Output Vessel with Correct Alignment

ii

M Marriott, Undergraduate Thesis

Appendix A.4

Input Vessel and Stent incorrectly aligned

Output Vessel with Incorrect Alignment

M Marriott, Undergraduate Thesis